Optical instabilities in Fabry-Perot resonators

Andrea Bassi, Franco Prati,* and Luigi A. Lugiato
Dipartimento di Scienza e Alta Tecnologia, Università dell'Insubria, Via Valleggio 11, 22100 Como, Italy

(Received 27 October 2020; revised 22 April 2021; accepted 27 April 2021; published 20 May 2021)

We start from the Maxwell-Bloch equations that govern the dynamics of Fabry-Perot lasers and, considering a doubled cavity, generalize our traveling wave formalism to the case in which the two-level medium does not fill the cavity but occupies only a portion of it. We linearize these equations and focus on the adiabatic elimination of both atomic fluctuations. Next, we restrict our attention to free running lasers under resonant conditions and analyze amplitude and phase instabilities. The examination of the unstable domain leads to the conclusion that the multimode Fabry-Perot instability arises near threshold only when the ratio of the longitudinal to the transverse atomic relaxation rate is substantially smaller than unity. This result agrees with our previous study in the limit of adiabatic elimination of the atomic polarization fluctuations only. We describe the self-pulsing behavior that arises from the multimode instability, and exhibits hysteretic behavior when the pump parameter is swept forward and backward. Finally, we investigate the single-mode instability and show that in the Fabry-Perot case there is no longer the correspondence between single-mode and multimode instabilities that is well known in the case of ring lasers. We confirm that in the case of resonant Fabry-Perot lasers the single-mode amplitude instability arises very far from threshold.

DOI: 10.1103/PhysRevA.103.053519

I. INTRODUCTION

The topic of instabilities and pattern formation in nonlinear materials contained in optical cavities represents a classic area of investigation in the vast domain of the dynamics of nonlinear systems, since the 1960s [1–6]. Presently, it is still a focus of attention thanks to the discoveries in the field of microresonator-based Kerr frequency combs [7–9] and the recent investigation on frequency combs in quantum cascade lasers (QCLs) [10–14].

A treatment of optical instabilities in lasers and related systems which includes coherent effects must be necessarily based on the Maxwell-Bloch equations (MBE). Given the complexity of such equations, however, the majority of investigations concern ring cavities because the field propagation is unidirectional. The case of Fabry-Perot (FP) cavities is substantially more complex because it involves two counterpropagating field envelopes. As a consequence, most of previous studies are purely numerical (see, e.g., Refs. [15–19]).

One simplifying assumption which is usually adopted in the study of mutimode instabilities in a FP cavity consists in keeping only the lower order spatial harmonics of the material variables, namely the zeroth- and second-order harmonics for the population inversion and the first-order (sometimes also the third-order [20]) harmonics for the polarization [21–25]. This assumption amounts to treating the problem at first order in the scaled stationary intensity of the single-mode solution, which limits the validity of the analysis to lasers close to threshold.

In a different context, related to the so-called Lugiato-Lefever equation, an analytic treatment of FP cavities was recently provided for both a Kerr medium [26] and a QCL [27].

Recently [28], two of us have introduced a traveling wave formalism (TWF) that substantially simplifies the problem of studying the instabilities of a FP cavity even for lasers well above threshold. Basically, we start from the MBE for the case of a FP cavity [29,30] and consider a cavity that occupies the interval $-L \leqslant z \leqslant 0$. We show that by considering the symmetrically doubled cavity in the interval $-L \leqslant z \leqslant L$ and appropriately defining the dynamical variables in the additional interval $0 \leqslant z \leqslant L$, it is possible to formulate the dynamical equations in terms of the forward-propagating envelope only.

In Ref. [28], the TWF has been introduced for the case in which the nonlinear two-level medium fills the cavity; one of the aims of the present paper is to extend it beyond this limitation. This generalization is important because that configuration is common and it is often used to vary the ratio of the cavity round-trip time to the gain recovery time, which is a very relevant quantity that determines if a laser is able to sustain self-pulsing. For instance, in QCLs, which have both very short recovery time and very short cavity length, an external cavity is often used to make the cavity round-trip time larger than the gain recovery time [31,32].

In a recent paper [33], the instabilities of a FP free running laser were studied in the limit of adiabatic elimination of the atomic polarization fluctuations only. In the present paper, we focus instead on the adiabatic elimination of both atomic fluctuations and present a stability analysis valid both for FP free running lasers and for FP cavities driven by an external coherent field.

*franco.prati@uninsubria.it

Next, we restrict our attention to free running FP lasers under resonance conditions and study amplitude and phase instabilities. We analyze the instability domain and solve numerically the dynamical equations in the TWF in order to describe the self-pulsing behavior that arises in the unstable region.

The main body of this article concerns multimode instabilities, i.e., instabilities that arise in modes different from the mode that corresponds to the homogeneous stationary solutions. The last section, however, is devoted to single-mode instabilities in FP lasers that correspond to the celebrated Lorenz-Haken instability in ring lasers. We perform this analysis basically to show that in the case of FP cavity there is no longer the correspondence between single- and multimode instabilities that holds in ring lasers [6], and we confirm the fact that the case of resonant FP lasers the single-mode amplitude instability is of no practical interest because this instability arises too far from threshold.

In Sec. II, we derive the modal equations for a Fabry-Perot cavity within the traveling wave formalism. In Sec. III, we perform the linear stability analysis of the single-mode stationary solutions and focus on the adiabatic elimination of the atomic fluctuations. Section IV is devoted to the analysis of amplitude and phase instabilities in the resonant configuration. We describe the instability domain and discuss numerical simulations and self-pulsing. In Sec. V, we analyze the Lorenz-Haken single-mode instability in FP lasers. Section VI concerns the conclusions of this paper.

II. MODAL EQUATIONS FOR A FABRY-PEROT CAVITY WITH THE TRAVELING-WAVE FORMALISM

Let us consider the Fabry-Perot (FP) cavity of length L shown in Fig. 1. It has mirrors with intensity transmissivity coefficient T (reflectivity $1-T$) and contains a two-level sample of length $\bar{L}$ much larger than a wavelength. The left facet of the sample is assumed to be antireflection coated in order to avoid internal reflections. $\mathcal{E}_I(t)$ is the monochromatic electric field injected into the cavity and $\mathcal{E}_T(t)$ is the transmitted field, where t denotes time. In the case of a free running laser, the incident field is absent and $\mathcal{E}_T(t)$ is the emitted field. The electric field along the cavity can be expressed as

$$\mathcal{E}(z,t) = \tfrac{1}{2}[\mathcal{E}_F(z,t) + \mathcal{E}_B(z,t) + \text{c.c.}], \tag{1}$$

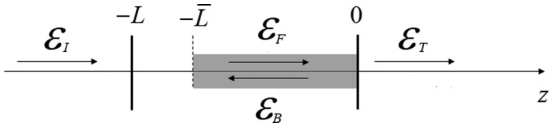

FIG. 1. A Fabry-Perot cavity is located in the interval $-L \leqslant z \leqslant 0$ and includes a two-level atom sample that occupies the portion $-\bar{L} \leqslant z \leqslant 0$. At $z = -L$ and $z = 0$, there are two mirrors with intensity transmissivity coefficient T. $\mathcal{E}_F$ and $\mathcal{E}_B$ denote the electric fields that propagate in the forward and backward directions, respectively. $\mathcal{E}_I$ and $\mathcal{E}_T$ are the input field and transmitted field, respectively.

where $\mathcal{E}_F$ and $\mathcal{E}_B$ include the factor $e^{-i\omega_0 t}$ and ω_0 denotes the carrier frequency. Since in the range $-L \leqslant z \leqslant -\bar{L}$ the electric field propagates in vacuum, we have at once that

$$\mathcal{E}_F(-\bar{L},t) = \mathcal{E}_F(-L, t-\Delta t), \tag{2a}$$
$$\mathcal{E}_B(-L,t) = \mathcal{E}_B(-\bar{L}, t-\Delta t), \tag{2b}$$

where Δt is the time the light takes to propagate from $-L$ to $-\bar{L}$ or vice versa, i.e., $\Delta t = (L-\bar{L})/c$, with c being the light velocity in vacuum. On the other hand, the boundary conditions at the mirrors, i.e., at $z = -L$ and $z = 0$ are, respectively,

$$\mathcal{E}_F(-L,t) = \sqrt{1-T}\,\mathcal{E}_B(-L,t) + \sqrt{T}\,\bar{\mathcal{E}}_I(t), \tag{3a}$$
$$\mathcal{E}_B(0,t) = \sqrt{1-T}\,\mathcal{E}_F(0,t), \tag{3b}$$
$$\bar{\mathcal{E}}_T(t) = \sqrt{T}\,\mathcal{E}_F(0,t), \tag{3c}$$

where $\bar{\mathcal{E}}_I$ and $\bar{\mathcal{E}}_T$ are such that

$$\mathcal{E}_I(t) = \tfrac{1}{2}[\bar{\mathcal{E}}_I(t) + \text{c.c.}], \tag{4a}$$
$$\mathcal{E}_T(t) = \tfrac{1}{2}[\bar{\mathcal{E}}_T(t) + \text{c.c.}]. \tag{4b}$$

By combining Eqs. (2) and (3a), we obtain

$$\mathcal{E}_F(-\bar{L},t) = \sqrt{1-T}\,\mathcal{E}_B(-\bar{L}, t-2\Delta t) + \sqrt{T}\,\bar{\mathcal{E}}_I(t-\Delta t). \tag{5}$$

Along the sample (i.e., for $-\bar{L} \leqslant z \leqslant 0$), we can set

$$\mathcal{E}_F(z,t) = E_F(z,t)e^{-i\omega_0 t + ik_0 z}, \tag{6a}$$
$$\mathcal{E}_B(z,t) = E_B(z,t)e^{-i\omega_0 t - ik_0 z}, \tag{6b}$$

where

$$k_0 = \frac{\omega_0}{\tilde{c}} = \frac{\omega_0 n_B}{c}, \tag{7}$$

$\tilde{c}$ denotes the light velocity in the sample, with n_B being the background refractive index, and $E_F(z,t)$, $E_B(z,t)$ are the slowly varying envelopes of the forward and backward propagating electric fields. We have also

$$\bar{\mathcal{E}}_I(t) = E_I(t)e^{-i\omega_0 t - ik_0 \bar{L}}, \tag{8a}$$
$$\bar{\mathcal{E}}_T(t) = E_T(t)e^{-i\omega_0 t}, \tag{8b}$$

where E_I and E_T denote the slowly varying envelope of the input and output fields. By inserting Eqs. (6) and (8a) into Eq. (5), we obtain

$$E_F(-\bar{L},t) = \sqrt{1-T}\,E_B(-\bar{L}, t-2\Delta t)e^{i\omega_0/(c/2\Lambda)} + \sqrt{T}E_I(t)e^{i\omega_0\Delta t}, \tag{9}$$

where $\Lambda = L - \bar{L} + n_B\bar{L}$ is the optical length of the cavity. In the same way, by combining Eqs. (3b) and (3c) with Eqs. (6) and (8), we obtain

$$E_B(0,t) = \sqrt{1-T}\,E_F(0,t), \tag{10a}$$
$$E_T(t) = \sqrt{T}E_F(0,t). \tag{10b}$$

Now we define

$$\delta_0 = 2\pi\bar{j} - \frac{\omega_0}{c/2\Lambda} = \frac{\omega_c - \omega_0}{c/2\Lambda}, \tag{11}$$

where the positive integer $\bar{j}$ is selected in such a way that the modulus of δ_0 is smaller than π, so that ω_c is the cavity frequency closest to the carrier frequency ω_0. We introduce

also the symbols

$$F_F(z,t)=\frac{dE_F(z,t)}{\hbar\sqrt{\gamma_\perp\gamma_\parallel}},\quad F_B(z,t)=\frac{dE_B(z,t)}{\hbar\sqrt{\gamma_\perp\gamma_\parallel}},\tag{12a}$$

$$x(t)=\frac{dE_T(t)}{\hbar\sqrt{\gamma_\perp\gamma_\parallel T}},\quad y(t)=\frac{dE_I(t)e^{i\omega_0\Delta t}}{\hbar\sqrt{\gamma_\perp\gamma_\parallel T}},\tag{12b}$$

where d is the modulus of the dipole moment and $\gamma_\perp$, $\gamma_\parallel$ are the relaxation rates of the atomic polarization and population difference of the two-level system, respectively. By using these definitions, we have

$$F_F(-\bar{L},t)=\sqrt{1-T}F_B(-\bar{L},t-2\Delta t)e^{-i\delta_0}+Ty,\tag{13a}$$

$$F_B(0,t)=\sqrt{1-T}F_F(0,t),\tag{13b}$$

$$x(t)=F_F(0,t),\tag{13c}$$

where we have assumed that the amplitude y of the injected field is time independent. Next, we turn our attention to the dynamical equations that govern the time evolution, that in the interval $-\bar{L}\leqslant z\leqslant 0$ are given by (see Eqs. (14.57)–(14.60) of Ref. [6])

$$\frac{\partial F_F(z,t)}{\partial z}+\frac{1}{\tilde{c}}\frac{\partial F_F(z,t)}{\partial t}=\frac{g}{2\pi}\int_{-\pi}^{\pi}d\varphi e^{-i\varphi}P(z,\varphi,t),\tag{14a}$$

$$-\frac{\partial F_B(z,t)}{\partial z}+\frac{1}{\tilde{c}}\frac{\partial F_B(z,t)}{\partial t}=\frac{g}{2\pi}\int_{-\pi}^{\pi}d\varphi e^{i\varphi}P(z,\varphi,t),\tag{14b}$$

$$\frac{\partial P(z,\varphi,t)}{\partial t}=\gamma_\perp[(F_F(z,t)e^{i\varphi}+F_B(z,t)e^{-i\varphi})\times D(z,\varphi,t)-(1+i\Delta)P(z,\varphi,t)],\tag{14c}$$

$$\frac{\partial D(z,\varphi,t)}{\partial t}=-\gamma_\parallel\left\{\frac{1}{2}[(F_F(z,t)e^{i\varphi}+F_B(z,t)e^{-i\varphi})\times P^*(z,\varphi,t)+\text{c.c.}]+D(z,\varphi,t)-1\right\},\tag{14d}$$

where $\varphi=k_0z$ and $P(z,\varphi,t)$, $D(z,\varphi,t)$ are the normalized atomic polarization and population difference, respectively. The symbol g denotes the atom-field coupling constant and $\Delta=(\omega_a-\omega_0)/\gamma_\perp$, where ω_a is the Bohr transition frequency of the two-level atoms. In the case of an absorbing medium instead of an amplifying medium, g must be replaced by $(-\alpha)$, where α is the absorption coefficient per unit length [6]. Equations (14) are associated with the boundary conditions (13a) and (13b). At this stage, let us introduce the following transformations:

$$F'_F(z,t)=e^{\frac{z}{2\bar{L}}[\ln(1-T)-i\delta_0]}F_F(z,t)+\frac{z}{2\bar{L}}\frac{Tye^{i\frac{\delta_0}{2}}}{\sqrt{1-T}},\tag{15a}$$

$$F'_B(z,t)=\frac{e^{-\frac{z}{2\bar{L}}[\ln(1-T)-i\delta_0]}}{\sqrt{1-T}}F_B(z,t)-\frac{z}{2\bar{L}}\frac{Tye^{i\frac{\delta_0}{2}}}{\sqrt{1-T}},\tag{15b}$$

where the transformed normalized envelopes $F'_F(z,t)$ and $F'_B(z,t)$ obey the boundary conditions

$$F'_F(-\bar{L},t)=F'_B(-\bar{L},t-2\Delta t),\tag{16a}$$

$$F'_F(0,t)=F'_B(0,t),\tag{16b}$$

and the low transmission limit [6] (also called mean field limit or uniform field limit in the literature)

$$T\ll 1,\quad |\delta_0|\ll 1,\quad g\bar{L}\ll 1,\tag{17}$$

with

$$\theta=\frac{\delta_0}{T}=O(1),\quad A=\frac{2g\bar{L}}{T}=O(1).\tag{18}$$

In this limit, Eqs. (14) become

$$\bar{L}\left(\frac{\partial F'_F(z,t)}{\partial z}+\frac{1}{\tilde{c}}\frac{\partial F'_F(z,t)}{\partial t}\right)=\frac{Ty}{2}\tag{19a}$$

$$-\frac{T+i\delta_0}{2}F'_F(z,t)+\frac{g\bar{L}}{2\pi}\int_{-\pi}^{\pi}d\varphi e^{-i\varphi}P(z,\varphi,t),$$

$$\bar{L}\left(-\frac{\partial F'_B(z,t)}{\partial z}+\frac{1}{\tilde{c}}\frac{\partial F'_B(z,t)}{\partial t}\right)=\frac{Ty}{2}\tag{19b}$$

$$-\frac{T+i\delta_0}{2}F'_B(z,t)+\frac{g\bar{L}}{2\pi}\int_{-\pi}^{\pi}d\varphi e^{i\varphi}P(z,\varphi,t),$$

$$\frac{\partial P(z,\varphi,t)}{\partial t}=\gamma_\perp[(F'_F(z,t)e^{i\varphi}+F'_B(z,t)e^{-i\varphi})\times D(z,\varphi,t)-(1+i\Delta)P(z,\varphi,t)],\tag{19c}$$

$$\frac{\partial D(z,\varphi,t)}{\partial t}=-\gamma_\parallel\left\{\frac{1}{2}[(F'_F(z,t)e^{i\varphi}+F'_B(z,t)e^{-i\varphi})\times P^*(z,\varphi,t)+\text{c.c.}]+D(z,\varphi,t)-1\right\}.\tag{19d}$$

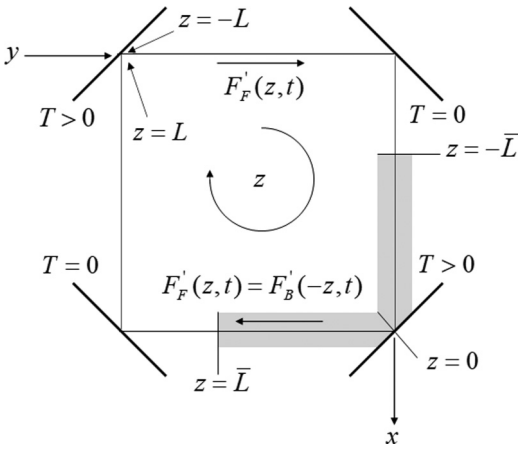

FIG. 2. The Fabry-Perot cavity of Fig. 1 is unfolded in a unidirectional ring cavity of length $2L$ from $-L$ to L with a two-level atoms sample that occupies the portion from $-\bar{L}$ to $\bar{L}$. At $z=-L$ and $z=0$, there are two mirrors with intensity transmissivity coefficient T while the other two mirrors are perfectly reflecting. The input beam enters the cavity at $z=-L$ and the output beams leaves the cavity at $z=0$. The intracavity field $F'_F(z,t)$ propagates clockwise, obeys periodic boundary conditions, and in the region of positive z coincides with the backward field of the Fabry-Perot cavity for negative z.

The traveling wave formalism for the dynamics of optical systems in nonlinear FP cavities [28] starts from symmetrically doubling the interval $-\bar{L} \leqslant z \leqslant 0$ to the interval $-\bar{L} \leqslant z \leqslant \bar{L}$, defining the quantities in play in the additional interval $0 \leqslant z \leqslant \bar{L}$ as follows:

$$F'_F(z,t) = F'_B(-z,t), \tag{20a}$$

$$F'_B(z,t) = F'_F(-z,t), \tag{20b}$$

and

$$P(z,\varphi,t) = P(-z,-\varphi,t), \tag{21a}$$

$$D(z,\varphi,t) = D(-z,-\varphi,t). \tag{21b}$$

We note that Eqs. (20) and (21) incorporate the boundary condition (16b) and are consistent with Eqs. (19) because, if in these equations we replace z and φ by $-z$ and $-\varphi$, respectively, and take into account Eqs. (20) and (21), we recover the starting set of equations (19). A scheme of the unfolded cavity is shown in Fig. 2.

The main advantage of the steps (20) and (21) is that now we can drop Eq. (19b), because $F'_B(z,t)$ is expressed in terms of $F'_F(z,t)$ using Eq. (20), and we can reformulate the set of dynamical equations as follows:

$$\bar{L}\left(\frac{\partial F'_F(z,t)}{\partial z} + \frac{1}{\tilde{c}}\frac{\partial F'_F(z,t)}{\partial t}\right) = \frac{Ty}{2} - \frac{T+i\delta_0}{2}F'_F(z,t) + \frac{g\bar{L}}{2\pi}\int_{-\pi}^{\pi} d\varphi e^{-i\varphi}P(z,\varphi,t), \tag{22a}$$

$$\frac{\partial P(z,\varphi,t)}{\partial t} = \gamma_\perp[(F'_F(z,t)e^{i\varphi} + F'_F(-z,t)e^{-i\varphi})D(z,\varphi,t) - (1+i\Delta)P(z,\varphi,t)], \tag{22b}$$

$$\frac{\partial D(z,\varphi,t)}{\partial t} = -\gamma_\parallel\left\{D(z,\varphi,t) - 1 + \frac{1}{2}[(F'_F(z,t)e^{i\varphi} + F'_F(-z,t)e^{-i\varphi})P^*(z,\varphi,t) + \text{c.c.}]\right\}. \tag{22c}$$

Grating in population inversion, which is typical of a FP cavity and causes spatial hole burning effects, is preserved even in the doubled cavity thanks to the combination $F'_F(z,t)e^{i\varphi} + F'_F(-z,t)e^{-i\varphi}$, which appears in the equations for the material variables P and D. Next, let us introduce the independent variable

$$\tau = t + \Delta t\frac{z}{\bar{L}}, \tag{23}$$

in terms of which Eq. (22a) becomes

$$\bar{L}\left(\frac{\partial F'_F(z,\tau)}{\partial z} + \frac{1}{c}\frac{\Lambda}{\bar{L}}\frac{\partial F'_F(z,\tau)}{\partial \tau}\right) = \frac{Ty}{2} - \frac{T+i\delta_0}{2}F'_F(z,\tau) + \frac{g\bar{L}}{2\pi}\int_{-\pi}^{\pi} d\varphi e^{-i\varphi}P(z,\varphi,\tau), \tag{24}$$

where we have taken into account the definitions of Δt and Λ given before. By introducing the field damping constant

$$k = \frac{cT}{2\Lambda} \tag{25}$$

and using Eq. (18), we arrive at the final form

$$c\frac{\bar{L}}{\Lambda}\frac{\partial F'_F(z,\tau)}{\partial z} + \frac{\partial F'_F(z,\tau)}{\partial \tau} = -k\left[(1+i\theta)F'_F(z,\tau) - y - \frac{A}{2\pi}\int_{-\pi}^{\pi} d\varphi e^{-i\varphi}P(z,\varphi,\tau)\right], \tag{26}$$

while the atomic equations (22b) and (22c) become

$$\frac{\partial P(z,\varphi,\tau)}{\partial \tau} = \gamma_\perp[(F'_F(z,\tau)e^{i\varphi} + F'_F(-z,\tau)e^{-i\varphi}) \times D(z,\varphi,\tau) - (1+i\Delta)P(z,\varphi,\tau)], \tag{27a}$$

$$\frac{\partial D(z,\varphi,\tau)}{\partial \tau} = -\gamma_\parallel\left\{D(z,\varphi,\tau) - 1 \times \frac{1}{2}[(F'_F(z,\tau)e^{i\varphi} + F'_F(-z,\tau)e^{-i\varphi}) \times P^*(z,\varphi,\tau) + \text{c.c.}]\right\}. \tag{27b}$$

In the case in which the two-level medium fills the cavity, i.e., $L = \bar{L}$, so that $\Delta t = 0$ and $\tau = t$, Eqs. (26) and (27) reduce to the dynamical equations (15)–(17) of Ref. [28]. In the general case, the time t is replaced by the variable τ defined by Eq. (23). In terms of the time τ, the boundary condition (16a) becomes

$$F'_F(-\bar{L},\tau) = F'_F(\bar{L},\tau), \tag{28}$$

where we have used Eqs. (20) and (23). Hence, $F'_F(z,\tau)$ obeys a periodic boundary condition in the interval $-\bar{L} \leqslant z \leqslant \bar{L}$.

On the basis of the periodic boundary condition, it is natural to introduce the expansion

$$F'_F(z,\tau) = \sum_{n=-\infty}^{+\infty} f_n(\tau)e^{i(n\pi/\bar{L})z}, \tag{29}$$

where

$$f_n(\tau) = \frac{1}{2\bar{L}}\int_{-\bar{L}}^{+\bar{L}} dz\, e^{-i(n\pi/\bar{L})z}F'_F(z,\tau) \tag{30}$$

and similarly

$$P(z,\varphi,\tau) = \sum_{n=-\infty}^{+\infty} p_n(\varphi,\tau)e^{i(n\pi/\bar{L})z}, \tag{31a}$$

$$D(z,\varphi,\tau) = \sum_{n=-\infty}^{+\infty} d_n(\varphi,\tau)e^{i(n\pi/\bar{L})z}. \tag{31b}$$

Equations (21) imply that

$$p_n(\varphi,\tau) = p_{-n}(-\varphi,\tau), \quad d_n(\varphi,\tau) = d_{-n}(-\varphi,\tau), \tag{32}$$

and, since $D(z, \varphi, \tau)$ is real, we have also

$$d_n^*(\varphi, \tau) = d_{-n}(\varphi, \tau). \tag{33}$$

If we insert Eqs. (29) and (31) into the dynamical equations (26) and (27) and take into account Eq. (30) and similar equations for $p_n(\varphi, \tau)$ and $d_n(\varphi, \tau)$, we obtain the following set of modal equations:

$$\frac{df_n(\tau)}{d\tau} = -i\alpha_n f_n(\tau) - k\left[(1+i\theta)f_n(\tau) - y\delta_{n,0} - \frac{A}{2\pi}\int_{-\pi}^{+\pi} d\varphi e^{-i\varphi} p_n(\varphi, \tau)\right], \tag{34a}$$

$$\gamma_\perp^{-1}\frac{\partial p_n(\varphi, \tau)}{\partial \tau} = \sum_{n'}[f_{n'}(\tau)d_{n-n'}(\varphi, \tau)e^{i\varphi} + f_{n'}(\tau)d_{n+n'}(\varphi, \tau)e^{-i\varphi}] - (1+i\Delta)p_n \times (\varphi, \tau), \tag{34b}$$

$$\gamma_\parallel^{-1}\frac{\partial d_n(\varphi, \tau)}{\partial \tau} = -\frac{1}{2}\sum_{n'}[f_{n'}(\tau)p^*_{n'-n}(\varphi, \tau)e^{i\varphi} + f_{n'}(\tau)p^*_{-n-n'}(\varphi, \tau)e^{-i\varphi} + f^*_{n'}(\tau)p_{n+n'}(\varphi, \tau)e^{-i\varphi} + f^*_{n'}(\tau)p_{n-n'}(\varphi, \tau)e^{i\varphi}] - [d_n(\varphi, \tau) - \delta_{n,0}], \tag{34c}$$

where $\delta_{n,0}$ is the Kronecker delta and n and n' are positive, null, or negative integers which run from $-\infty$ to $+\infty$ and

$$\alpha_n = \frac{\pi c}{\Lambda} n. \tag{35}$$

The parameter α_n is the frequency difference between the nth side mode and the resonant mode, and α_1 is the free spectral range of the cavity. Equations (34) and (35) coincide with Eqs. (24)–(28) of Ref. [28], but are more general in that they describe a FP laser where the active medium occupies only a part of the cavity while in Ref. [28] the medium was assumed to fill completely the cavity. In that case, $\Lambda = n_B L$ so that Eq. (35) coincides with Eq. (27) of Ref. [28].

III. LINEAR STABILITY ANALYSIS OF THE SINGLE-MODE SOLUTION

Let us now consider a uniform stationary single-mode solution of Eqs. (34). In correspondence with such a solution, the values of the modal amplitudes are

$$f_n = f\delta_{n,0}, \quad p_n(\varphi) = p(\varphi)\delta_{n,0}, \quad d_n(\varphi) = d(\varphi)\delta_{n,0}, \tag{36}$$

where $p(\varphi)$ and $d(\varphi)$ are given by

$$d(\varphi) = \frac{1+\Delta^2}{1+\Delta^2+4\cos^2\varphi\,|f|^2}, \tag{37a}$$

$$p(\varphi) = \frac{2\cos\varphi(1-i\Delta)}{1+\Delta^2+4\cos^2\varphi\,|f|^2} f, \tag{37b}$$

and f obeys the equation

$$y = (1+i\theta)f - \frac{A}{2\pi}\int_{-\pi}^{\pi} d\varphi e^{-i\varphi} p(\varphi). \tag{38}$$

Since $p(\varphi)$ is an even function of φ, in Eq. (38) we can replace $e^{-i\varphi}$ by $\cos\varphi$. By introducing the expression (37b) of $p(\varphi)$ into Eq. (38), the integral over φ can be performed analytically (see Eqs. (14.47)–(14.49) of Ref. [6]) and the result is the stationary equation

$$y = f\left\{1 + i\theta - \frac{A(1-i\Delta)}{2|f|^2}\left[1 - \frac{1}{\sqrt{1+\frac{4|f|^2}{1+\Delta^2}}}\right]\right\}. \tag{39}$$

We do not discuss Eq. (39) in the general case; we simply assume that its stationary solution f has been calculated. If we write now

$$f_n(\tau) = f\delta_{n,0} + \delta f_n(\tau), \tag{40a}$$

$$p_n(\varphi, \tau) = p(\varphi)\delta_{n,0} + \delta p_n(\varphi, \tau), \tag{40b}$$

$$d_n(\varphi, \tau) = d(\varphi)\delta_{n,0} + \delta d_n(\varphi, \tau), \tag{40c}$$

the linearized equations read

$$\frac{d\delta f_n(\tau)}{d\tau} = -i\alpha_n\delta f_n(\tau) - k\left[(1+i\theta)\delta f_n(\tau) - \frac{A}{2\pi}\int_{-\pi}^{+\pi} d\varphi e^{-i\varphi}\delta p_n(\varphi, \tau)\right], \tag{41a}$$

$$\gamma_\perp^{-1}\frac{\partial \delta p_n(\varphi, \tau)}{\partial \tau} = -(1+i\Delta)\delta p_n(\varphi, \tau) + [\delta f_n(\tau)e^{i\varphi} + \delta f_{-n}(\tau)e^{-i\varphi}]d(\varphi) + 2f\cos\varphi\,\delta d_n(\varphi, \tau), \tag{41b}$$

$$\gamma_\parallel^{-1}\frac{\partial \delta d_n(\varphi, \tau)}{\partial \tau} = -\delta d_n(\varphi, \tau) - \frac{1}{2}\{[\delta f_n(\tau)e^{i\varphi} + \delta f_{-n}(\tau)e^{-i\varphi}]p^*(\varphi) + [\delta f^*_{-n}(\tau)e^{-i\varphi} + \delta f^*_n(\tau)e^{i\varphi}]p(\varphi) + 2\cos\varphi[f\delta p^*_{-n}(\varphi, \tau) + f^*\delta p_n(\varphi, \tau)]\}. \tag{41c}$$

A. Adiabatic elimination of the atomic fluctuations

In order to perform the adiabatic elimination of the atomic fluctuations δp_n and δd_n, it is convenient to introduce the following transformations:

$$\delta f_n(\tau) = \delta\tilde{f}_n(\tau)e^{-i\alpha_n\tau}, \tag{42a}$$

$$\delta p_n(\varphi, \tau) = \delta\tilde{p}_n(\varphi, \tau)e^{-i\alpha_n\tau}, \tag{42b}$$

$$\delta d_n(\varphi, \tau) = \delta\tilde{d}_n(\varphi, \tau)e^{-i\alpha_n\tau}, \tag{42c}$$

so that Eqs. (41) become

$$\frac{d\delta\tilde{f}_n(\tau)}{d\tau} = -k\left[(1+i\theta)\delta\tilde{f}_n(\tau) - \frac{A}{2\pi}\int_{-\pi}^{+\pi} d\varphi e^{-i\varphi}\delta\tilde{p}_n(\varphi, \tau)\right], \tag{43a}$$

$$\gamma_\perp^{-1}\frac{\partial\delta\tilde{p}_n(\varphi,\tau)}{\partial\tau} = -\left(1+i\Delta-i\frac{\alpha_n}{\gamma_\perp}\right)\delta\tilde{p}_n(\varphi,\tau) + [\delta\tilde{f}_n(\tau)e^{i\varphi}+\delta\tilde{f}_{-n}(\tau)e^{-i\varphi}e^{2i\alpha_n\tau}]d(\varphi) + 2f\cos\varphi\,\delta\tilde{d}_n(\varphi,\tau), \tag{43b}$$

$$\gamma_\parallel^{-1}\frac{\partial\delta d_n(\varphi,\tau)}{\partial\tau} = -\left(1-i\frac{\alpha_n}{\gamma_\parallel}\right)\delta\tilde{d}_n(\varphi,\tau) - \frac{1}{2}\{[\delta\tilde{f}_n(\tau)e^{i\varphi}+\delta\tilde{f}_{-n}(\tau)e^{-i\varphi}e^{2i\alpha_n\tau}]p^*(\varphi) + [\delta\tilde{f}^*_{-n}(\tau)e^{-i\varphi}+\delta\tilde{f}^*_n(\tau)e^{i\varphi}e^{2i\alpha_n\tau}]p(\varphi) + 2\cos\varphi[f\delta\tilde{p}^*_{-n}(\varphi,\tau)+f^*\delta\tilde{p}_n(\varphi,\tau)]\}. \tag{43c}$$

A relevant feature is that some (but not all) of the terms that originate from the backward field $F_B(z,\tau)=F_F(-z,\tau)$ display a time-dependent exponential.

In the framework of the linear stability analysis of a uniform stationary solution, in the regime of adiabatic elimination of the atomic fluctuations, identified by the condition

$$k \ll \gamma_\perp, \gamma_\parallel, \tag{44}$$

which defines a class-A laser, we consider instabilities which arise only in modes different from the resonant one and in the linearized equations (43) we assume $n\neq 0$. In the limit (44), the field fluctuations $\delta\tilde{f}_n$ can be considered slow variables, while the atomic fluctuations $\delta\tilde{p}_n$ and $\delta\tilde{d}_n$ can be considered fast variables and can be adiabatically eliminated by dropping the derivative term in Eqs. (43b) and (43c). Once this is done, the atomic amplitudes become functions of the slow variables and vary in time with the slow temporal scale k^{-1}. Therefore, if in Eqs. (43b) and (43c) without the derivative term we integrate the right-hand side over a τ interval much smaller than k^{-1} but much larger than α_1^{-1}, all terms remain practically unchanged, with the exception of the terms that include a time-varying exponential, which vanish, and Eqs. (43b) and (43c) without time derivatives reduce to

$$0 = i\alpha_n\delta\tilde{p}_n(\varphi,\tau)-\gamma_\perp(1+i\Delta)\delta\tilde{p}_n(\varphi,\tau)+\gamma_\perp[\delta\tilde{f}_n(\tau)e^{i\varphi}d(\varphi)+2f\cos\varphi\,\delta\tilde{d}_n(\varphi,\tau)], \tag{45a}$$

$$0 = (i\alpha_n-\gamma_\parallel)\delta\tilde{d}_n(\varphi,\tau)-\frac{\gamma_\parallel}{2}\{\delta\tilde{f}_n(\tau)e^{i\varphi}p^*(\varphi)+\delta\tilde{f}^*_{-n}(\tau)e^{-i\varphi}p(\varphi)+2\cos\varphi[f\delta\tilde{p}^*_{-n}(\varphi,\tau)+f^*\delta\tilde{p}_n(\varphi,\tau)]\}. \tag{45b}$$

In addition to Eqs. (43a) and (45), we must consider the equations

$$\frac{d\delta\tilde{f}^*_{-n}(\tau)}{d\tau} = -k\left[(1-i\theta)\delta\tilde{f}^*_{-n}(\tau)-\frac{A}{2\pi}\int_{-\pi}^{+\pi}d\varphi e^{i\varphi}\delta\tilde{p}^*_{-n}(\varphi,\tau)\right], \tag{46a}$$

$$0 = i\alpha_n\delta\tilde{p}^*_{-n}(\varphi,\tau)-\gamma_\perp(1-i\Delta)\delta\tilde{p}^*_{-n}(\varphi,\tau)+\gamma_\perp[\delta\tilde{f}^*_{-n}(\tau)e^{-i\varphi}d(\varphi)+2f^*\cos\varphi\,\delta\tilde{d}_n(\varphi,\tau)], \tag{46b}$$

that are obtained from Eqs. (43a) and (45a) by performing the complex conjugation, replacing n by $(-n)$, and taking Eq. (33) into account. The algebraic equations (45a), (46b), and (45b) can be solved with respect to $\delta\tilde{p}_n(\varphi,\tau)$, $\delta\tilde{p}^*_{-n}(\varphi,\tau)$, and $\delta\tilde{d}_n(\varphi,\tau)$ to find the expressions of $\delta\tilde{p}_n(\varphi,\tau)$ and $\delta\tilde{p}^*_{-n}(\varphi,\tau)$ as a function of $\delta f_n(\tau)$ and $\delta f^*_{-n}(\tau)$. In order to write these expressions, we note that Eqs. (45a), (46b), and (45b) are identical to Eqs. (20.12)–(20.14) of Ref. [6] with the time derivatives set equal to zero, provided in the latter equations one replaces $\delta\tilde{f}_n$ by $\delta\tilde{f}_n e^{i\varphi}$ and x by $2f\cos\varphi$. Also, the expressions (37) of $p(\varphi)$ and $d(\varphi)$ are obtained from the expressions of $\tilde{d}_{0,s}$ and $\tilde{p}_{0,s}$, that appear in Eqs. (20.12)–(20.14) of Ref. [6], by replacing x by $2f\cos\varphi$. Therefore, by following the procedure outlined at the beginning of Sec. 20.2 of Ref. [6], we can write

$$\delta\tilde{p}_n(\varphi,\tau) = T_1(\tilde{\alpha}_n,|f|^2\cos^2\varphi,\Delta,\tilde{\gamma})\delta\tilde{f}_n(\tau)e^{i\varphi}+T_2(\tilde{\alpha}_n,|f|^2\cos^2\varphi,\Delta,\tilde{\gamma})4f^2\cos^2\varphi\delta\tilde{f}_{-n}(\tau)^*e^{-i\varphi}, \tag{47a}$$

$$\delta\tilde{p}^*_{-n}(\varphi,\tau) = T_2(\tilde{\alpha}_n,|f|^2\cos^2\varphi,-\Delta,\tilde{\gamma})4f^{*2}\cos^2\varphi\,\delta\tilde{f}_n(\tau)e^{i\varphi}+T_1(\tilde{\alpha}_n,|f|^2\cos^2\varphi,-\Delta,\tilde{\gamma})\delta\tilde{f}^*_{-n}e^{-i\varphi}, \tag{47b}$$

where

$$\tilde{\alpha}_n=\frac{\alpha_n}{\gamma_\perp},\quad \tilde{\gamma}=\frac{\gamma_\parallel}{\gamma_\perp} \tag{48}$$

and the symbols T_1 and T_2 are defined as follows:

$$T_1(\tilde{\alpha}_n,|f|^2\cos^2\varphi,\Delta,\tilde{\gamma}) = B\frac{(1+\Delta^2)(1-i\tilde{\alpha}_n-i\Delta)-i\Gamma\tilde{\alpha}_n(1+i\Delta)4|f|^2\cos^2\varphi}{(1-i\tilde{\alpha}_n)(1-i\tilde{\alpha}_n-8\Gamma|f|^2\cos^2\varphi)+\Delta^2}, \tag{49a}$$

$$T_2(\tilde{\alpha}_n,|f|^2\cos^2\varphi,\Delta,\tilde{\gamma}) = B\frac{\Gamma(1-i\Delta)(2-i\tilde{\alpha}_n)}{(1-i\tilde{\alpha}_n)(1-i\tilde{\alpha}_n-8\Gamma|f|^2\cos^2\varphi)+\Delta^2}, \tag{49b}$$

with Γ and B given by

$$\Gamma=\frac{1}{2}\frac{\tilde{\gamma}}{i\tilde{\alpha}_n-\tilde{\gamma}},\quad B=\frac{1}{1+\Delta^2+4|f|^2\cos^2\varphi}. \tag{50}$$

By inserting Eqs. (47) into Eqs. (43a) and (46a), we arrive finally at the two equations

$$\frac{d\delta\tilde{f}_n(\tau)}{d\tau} = -k\Big\{(1+i\theta)\delta f_n - \frac{A}{2\pi}\int_{-\pi}^{+\pi} d\varphi[T_1(\tilde{\alpha}_n, |f|^2\cos^2\varphi, \Delta, \tilde{\gamma})\delta\tilde{f}_n(\tau) + T_2(\tilde{\alpha}_n, |f|^2\cos^2\varphi, \Delta, \tilde{\gamma}) \times 4f^2\cos^2\varphi(2\cos^2\varphi - 1)\delta\tilde{f}^*_{-n}(\tau)]\Big\}, \tag{51a}$$

$$\frac{d\delta\tilde{f}^*_{-n}(\tau)}{d\tau} = -k\Big\{(1-i\theta)\delta f^*_{-n} - \frac{A}{2\pi}\int_{-\pi}^{+\pi} d\varphi[T_2(\tilde{\alpha}_n, |f|^2\cos^2\varphi, -\Delta, \tilde{\gamma})4f^{*2}\cos^2\varphi(2\cos^2\varphi - 1)\delta\tilde{f}_n(\tau) \times T_1(\tilde{\alpha}_n, |f|^2\cos^2\varphi, -\Delta, \tilde{\gamma})\delta\tilde{f}^*_{-n}(\tau)]\Big\}, \tag{51b}$$

where, since T_1 and T_2 are even functions of φ, we have replaced $e^{\pm 2i\varphi}$ by $\cos(2\varphi) = 2\cos^2\varphi - 1$. These equations are general and allow us to study the stability of active and passive systems, with or without a driving field, with an atomic and cavity detuning. In the rest of the paper, however, we focus on the case of a free running laser ($y = 0$) and assume perfect resonance between the lasing mode and the cavity ($\theta = 0$) and the atoms ($\Delta = 0$).

IV. THE RESONANT LASER: AMPLITUDE AND PHASE INSTABILITIES

A. Stationary solution and gain functions

In the case of a resonant laser, we can assume without loss of generality that the stationary field amplitude f is real. The stationary intensity $X = f^2$ can be found by inverting the relation

$$A = \frac{2X\sqrt{1+4X}}{\sqrt{1+4X}-1}. \tag{52}$$

Unlike in a ring laser, the relation between the pump parameter A and the stationary intensity is nonlinear. It becomes linear only in the limit $X \ll 1$ where $A \approx 1 + 3X$. Since in the following analysis the term $\sqrt{1+4X}$ appears frequently in the formulas, we will often use the auxiliary function

$$R = \sqrt{1+4X}, \tag{53}$$

instead of X. In terms of R, for instance, the stationary solution reads

$$A = R(R+1)/2. \tag{54}$$

At the lasing threshold $X = 0$, $R = 1$, and $A = 1$.

In a resonant laser, Eqs. (51a) and (51b) can be decoupled by defining the new fluctuations

$$\delta f_{n\pm} = \delta f_n \pm \delta f^*_{-n}. \tag{55}$$

The equations for the new variables are

$$\frac{d\tilde{f}_{n\pm}(\tau)}{d\tau} = -k\Big\{1 - \frac{A}{2\pi}\int_{-\pi}^{+\pi} d\varphi[T_1(\tilde{\alpha}_n, |f|^2\cos^2\varphi, 0, \tilde{\gamma}) \pm T_2(\tilde{\alpha}_n, |f|^2\cos^2\varphi, 0, \tilde{\gamma}) \times 4X\cos^2\varphi(2\cos^2\varphi - 1)]\Big\}\delta\tilde{f}_{n\pm}(\tau). \tag{56}$$

The equations can be written as

$$\frac{d\delta\tilde{f}_{n\pm}(\tau)}{d\tau} = -k\{1 - A[H_1(\tilde{\alpha}_n, X, \tilde{\gamma}) \pm H_2(\tilde{\alpha}_n, X, \tilde{\gamma})X]\}\delta\tilde{f}_{n\pm}(\tau), \tag{57}$$

by defining the integrals

$$H_1(\tilde{\alpha}_n, X, \tilde{\gamma}) = \frac{1}{2\pi}\int_{-\pi}^{+\pi} d\varphi\, T_1(\tilde{\alpha}_n, X\cos^2\varphi, 0, \tilde{\gamma}), \tag{58a}$$

$$H_2(\tilde{\alpha}_n, X, \tilde{\gamma}) = \frac{1}{2\pi}\int_{-\pi}^{+\pi} d\varphi\, 4\cos^2\varphi(2\cos^2\varphi - 1) \times T_2(\tilde{\alpha}_n, X\cos^2\varphi, 0, \tilde{\gamma}). \tag{58b}$$

If we set

$$\delta\tilde{f}_{n\pm}(\tau) = e^{\lambda\tau}\delta f_{n\pm}, \tag{59}$$

we obtain a simple expression for the two eigenvalues

$$\lambda_\pm = k\{A[H_1(\tilde{\alpha}_n, X, \tilde{\gamma}) \pm H_2(\tilde{\alpha}_n, X, \tilde{\gamma})X] - 1\}. \tag{60}$$

A multimode instability arises when the real part of λ_+ or λ_- is positive for some values of n different from zero or, equivalently, when one of the two gain functions

$$\mathcal{G}_\pm(\tilde{\alpha}_n, X, \tilde{\gamma}) = A\mathrm{Re}[H_1(\tilde{\alpha}_n, X, \tilde{\gamma}) \pm H_2(\tilde{\alpha}_n, X, \tilde{\gamma})X] \tag{61}$$

becomes larger than unity. We can fix X and $\tilde{\gamma}$ and plot $\mathcal{G}_+$ and $\mathcal{G}_-$ as a function of $\tilde{\alpha}_n$ treated as a continuous variable. If there is an interval $\tilde{\alpha}_{n,\min} < \tilde{\alpha}_n < \tilde{\alpha}_{n,\max}$ where $\mathcal{G}_+ > 1$ or $\mathcal{G}_- > 1$, a multimode instability is present if for at least one value of n (or, more precisely, for at least one pair of values $\pm n$, since $\mathcal{G}_+$ and $\mathcal{G}_-$ are even functions of $\tilde{\alpha}_n$) $\tilde{\alpha}_n$ lies in the interval $\tilde{\alpha}_{n,\min} < \tilde{\alpha}_n < \tilde{\alpha}_{n,\max}$. Alternatively, we can fix $\tilde{\gamma}$ and draw in the $(X, \tilde{\alpha}_n)$ the boundary of the two instability domain given by the conditions $\mathcal{G}_\pm(\tilde{\alpha}_n, X, \tilde{\gamma}) = 1$.

The analytic expressions for the integrals $H_1(\tilde{\alpha}_n, X, \tilde{\gamma})$ and $H_2(\tilde{\alpha}_n, X, \tilde{\gamma})$ can be found in Appendix A. In the following, we will express the gain functions in terms of R instead of X.

In the limit $\tilde{\gamma} \to 0$, the two gain functions coincide because $H_2(\tilde{\alpha}_n, X, 0) = 0$, and we have

$$\mathcal{G}_\pm(\tilde{\alpha}_n, R, 0) = \frac{R+1}{2}\frac{1}{1+\tilde{\alpha}_n^2}. \tag{62}$$

The instability condition in this limit reads

$$0 \leqslant \tilde{\alpha}_n < \sqrt{\frac{R-1}{2}}. \tag{63}$$

The limit $\tilde{\gamma} \to 0$ with $\tilde{\alpha}_n$ finite is equivalent to the condition $\gamma_\parallel \ll \alpha_n$. If we look at Eq. (45b), we see that this condition amounts to setting $\delta\tilde{d}_n = 0$, i.e., neglecting the so-called *population pulsations* or else neglecting coherent effects. For that reason, in Ref. [23] the instability arising in that limit was named *incoherent instability*.

We also note that Eq. (63) coincides with the instability domain found in the case of adiabatic elimination of the fluctuations of the atomic polarization only in Ref. [33]. The conditions for this adiabatic elimination are $k \ll \gamma_\perp$, $\gamma_\parallel \ll \gamma_\perp$, $\gamma_\parallel \ll \alpha_n$ with $k/\gamma_\parallel$ arbitrary, whereas the conditions for the adiabatic elimination of both atomic fluctuations are $k \ll \gamma_\perp$, $k \ll \gamma_\parallel$ with $\gamma_\parallel/\gamma_\perp$ arbitrary. Hence, the parametric domain $k \ll \gamma_\perp$, $k \ll \gamma_\parallel$, $\gamma_\parallel \ll \gamma_\perp$, $\gamma_\parallel \ll \alpha_n$ is common to both adiabatic eliminations.

As soon as $\tilde{\gamma}$ is larger than zero, the two gain functions differ, and they can be written as

$$\mathcal{G}_+(\tilde{\alpha}_n, R, \tilde{\gamma}) = \mathcal{F}_1(\tilde{\alpha}_n, R, \tilde{\gamma}) + \mathcal{F}_2(\tilde{\alpha}_n, R, \tilde{\gamma}), \tag{64}$$

$$\mathcal{G}_-(\tilde{\alpha}_n, R, \tilde{\gamma}) = -\mathcal{F}_1(\tilde{\alpha}_n, R, \tilde{\gamma}) - R^2\mathcal{F}_2(\tilde{\alpha}_n, R, \tilde{\gamma}) + \mathcal{F}_3(\tilde{\alpha}_n, R, \tilde{\gamma}), \tag{65}$$

where the auxiliary functions $\mathcal{F}_{1,2,3}(\tilde{\alpha}_n, R, \tilde{\gamma})$ are defined as

$$\mathcal{F}_1(\tilde{\alpha}_n, R, \tilde{\gamma}) = \frac{R}{2}\left(\frac{S_+ - 1}{R-1} + \frac{1}{1+\tilde{\alpha}_n^2}\right), \tag{66}$$

$$\mathcal{F}_2(\tilde{\alpha}_n, R, \tilde{\gamma}) = \frac{RS_-}{\tilde{\alpha}_n(R-1)} + \frac{\tilde{\alpha}_n(1-\tilde{\gamma})(RS_+ - 1) - RS_-\left(2 + 2\tilde{\gamma} + \tilde{\alpha}_n^2\right)}{2\tilde{\alpha}_n(R-1)\left[(\tilde{\gamma}+1)^2 + \tilde{\alpha}_n^2\right]}, \tag{67}$$

$$\mathcal{F}_3(\tilde{\alpha}_n, R, \tilde{\gamma}) = \frac{(R+1)(RS_+ + \tilde{\alpha}_n RS_- + 1)}{2(1+\tilde{\alpha}_n^2)}, \tag{68}$$

with

$$S_\pm = \frac{1}{\sqrt{2p_1}}\sqrt{\sqrt{\left(1+\tilde{\alpha}_n^2\right)\left(\tilde{\gamma}^2 + \tilde{\alpha}_n^2\right)}p_1 \pm p_2}, \tag{69}$$

$$p_1 = \left(\tilde{\alpha}_n^2 - \tilde{\gamma}R^2\right)^2 + (1+\tilde{\gamma})^2\tilde{\alpha}_n^2, \tag{70}$$

$$p_2 = p_1 + \tilde{\gamma}(R^2-1)\left(\tilde{\alpha}_n^2 - \tilde{\gamma}R^2\right). \tag{71}$$

We note that in the limit $\tilde{\gamma} \to 0$, we have $S_+ = 1$, $S_- = 0$ and therefore $\mathcal{F}_1 = R/[2(1+\tilde{\alpha}_n^2)]$, $\mathcal{F}_2 = 1/[2(1+\tilde{\alpha}_n^2)]$, and $\mathcal{F}_3 = (R+1)^2/[2(1+\tilde{\alpha}_n^2)]$, and one can check easily that both Eqs. (64) and (65) reduce to Eq. (62).

The instability associated with $\mathcal{G}_+$ is an amplitude instability, while the instability associated with $\mathcal{G}_-$ is a phase instability. The reason for this terminology is clear from the definition (55) of the fluctuations $\delta f_{n\pm}$. When the stationary solution is unstable against δf_{n+} two symmetric *in-phase* modes grow. Apart from a global phase, the electric field is real. Conversely, when the instability is caused by the fluctuation δf_{n-} the two symmetric modes that grow are *out of phase* and the phase dynamics of the total field can no longer be neglected. In Refs. [22,23,25], the two kinds of instability were named, respectively, AM and FM instability.

We note that in the limit of adiabatic elimination of atomic polarization fluctuations only [33], the boundaries of amplitude and phase instability in the $(R, \tilde{\alpha}_n)$ plane coincide.

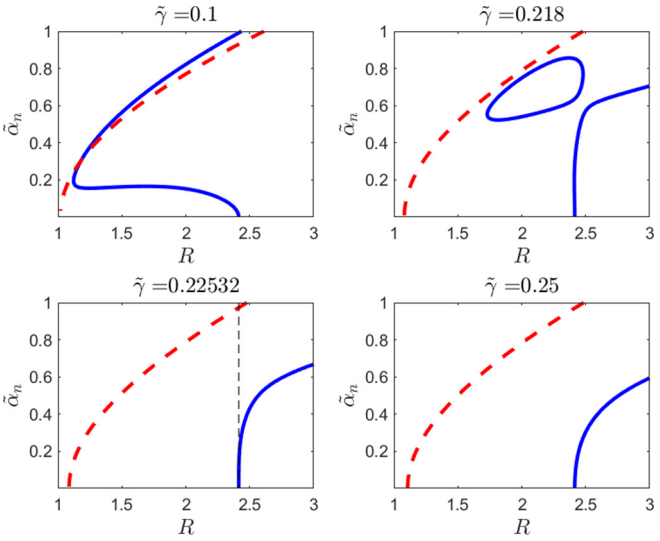

FIG. 3. Amplitude (solid blue line) and phase (dashed red line) instability domains in the plane $(R, \tilde{\alpha}_n)$ for the reported values of $\tilde{\gamma}$ of order 0.1. The boundary of the amplitude instability domain always intersects the axis $\tilde{\alpha}_n = 0$ in $R = R_c = 1 + \sqrt{2}$. For $\tilde{\gamma} = 0.22532$ in that point the curve has a vertical tangent, displayed as a thin dashed black line.

B. Instability domains

In Figs. 3 and 4, we show some examples of instability domains for the amplitude and phase instability in the plane $(R, \tilde{\alpha}_n)$ and for various values of $\tilde{\gamma}$ of order 0.1 (Fig. 3) and 1 (Fig. 4).

In order to understand those graphs, it is useful to study the behavior of the functions $\mathcal{G}_\pm(\tilde{\alpha}_n, R, \tilde{\gamma})$ in the limit $\tilde{\alpha}_n \to 0$. Since the laser is resonant with a cavity mode and with the atoms, the instability domains are symmetric with respect to the central mode and the functions $\mathcal{G}_\pm(\tilde{\alpha}_n, R, \gamma)$ are polynomials that contain only even powers of $\tilde{\alpha}_n$. At the lowest orders, we can write

$$\mathcal{G}_+(\tilde{\alpha}_n, R, \tilde{\gamma}) \approx \frac{R^3 - R^2 + R + 1}{2R^2} + \left[(R-1)\frac{R^4(1-\tilde{\gamma}) + R^2(4+11\tilde{\gamma}+\tilde{\gamma}^2) - 5(1+\tilde{\gamma})^2}{16R^6\tilde{\gamma}^2} - \frac{R}{2}\right]\tilde{\alpha}_n^2, \tag{72}$$

$$\mathcal{G}_-(\tilde{\alpha}_n, R, \tilde{\gamma}) \approx 1 + \left[(R-1)\frac{R^4(1+\tilde{\gamma}-10\tilde{\gamma}^2) + R^2(1-\tilde{\gamma})\tilde{\gamma} - (1+\tilde{\gamma})^2}{16R^4\tilde{\gamma}^2} + \frac{R}{2}\right]\alpha_n^2. \tag{73}$$

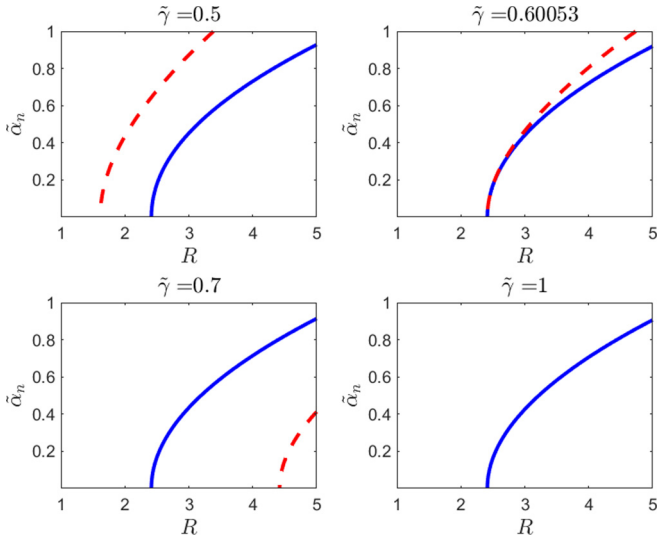

FIG. 4. Amplitude (solid blue line) and phase (dashed red line) instability domains in the plane $(R, \tilde{\alpha}_n)$ for the reported values of $\tilde{\gamma}$ of order 1. The point where the boundary of the phase instability domain intersects the axis $\tilde{\alpha}_n = 0$ grows rapidly with $\tilde{\gamma}$ and both boundaries intersects the axis at $R = R_c = 1 + \sqrt{2}$ when $\tilde{\gamma} = 0.60053$. For $\tilde{\gamma} \geqslant 1$, there is no phase instability.

Let us consider first $\mathcal{G}_+(\tilde{\alpha}_n, R, \tilde{\gamma})$. In the exact limit $\tilde{\alpha}_n = 0$, the condition $\mathcal{G}_+(0, R, \tilde{\gamma}) > 1$ is independent of $\tilde{\gamma}$ and it is equivalent to $R > R_c$, with

$$R_c = 1 + \sqrt{2} = 2.414\ldots. \tag{74}$$

According to Eq. (54), this corresponds to the critical value for the pump parameter

$$A_c = 2 + 3/\sqrt{2} = 4.121\ldots. \tag{75}$$

This explains why the boundary of the amplitude instability domain always intersects the axis $\tilde{\alpha}_n = 0$ at the same point $R = R_c$, a feature clearly visible in the graphs of Figs. 3 and 4.

Looking at the graphs of Fig. 3, we also see that for small $\tilde{\alpha}_n$ the amplitude instability domains extends to the left of R_c for the smaller values of $\tilde{\gamma}$ and to the right for the larger. This depends on the sign of the coefficient of $\tilde{\alpha}_n^2$ in $\mathcal{G}_+$. For $R = R_c$, the single-mode stationary solution is unstable for positive values of that coefficient and stable otherwise. The critical value of $\tilde{\gamma}$ which discriminates between the two behaviors can be found by setting equal to zero the expression for the coefficient with $R = R_c$. In that way, we obtain a second-order equation in $\tilde{\gamma}$ whose positive solution is

$$\tilde{\gamma}_c = 0.22532\ldots. \tag{76}$$

As shown in the left lower graph of Fig. 3, for that value of $\tilde{\gamma}$ the curve of the amplitude instability boundary has a vertical tangent in $R = R_c$. It is also interesting to observe that when approaching $\tilde{\gamma}_c$ from below the amplitude instability domain splits in two parts.

The gain function $\mathcal{G}_-(\tilde{\alpha}_n, R, \tilde{\gamma})$ has a different behavior because it is identically equal to 1 for $\tilde{\alpha}_n = 0$. This means that the single-mode stationary solution is unstable versus the phase instability if the coefficient of $\tilde{\alpha}_n^2$ in $\mathcal{G}_+$ is positive and stable otherwise.

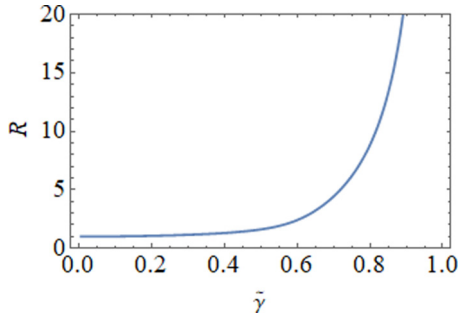

FIG. 5. This curve establishes the link between the parameter $\tilde{\gamma}$ and the value of R at which the boundary of the phase instability domain intersects the axis $\tilde{\alpha}_n = 0$. For $\tilde{\gamma} > 1$, there is no intersection.

By setting equal to zero that coefficient, we find an equation that links $\tilde{\gamma}$ with the value of R at which the phase instability domain intersects the axis $\tilde{\alpha}_n = 0$. Again, the condition is a second-order equation in $\tilde{\gamma}$ whose positive solution gives the desired relationship.

The plot of R as a function of $\tilde{\gamma}$ is shown in Fig. 5. At the beginning R grows very slowly with $\tilde{\gamma}$, but when $\tilde{\gamma}$ approaches 1 the curve tends rapidly to infinity. This explains why the point where the boundary of the phase instability domain intersects the axis $\tilde{\alpha}_n = 0$ grows slowly with $\tilde{\gamma}$ in the plots of Fig. 3 and much more rapidly in Fig. 4, and in the right lower graph of that figure there is no phase instability. The value of $\tilde{\gamma}$ in the right upper graph of Fig. 4 is the one associated with R_c; for that $\tilde{\gamma}$ both curves intersect the axis $\tilde{\alpha}_n = 0$ in $R = R_c$. We can also observe that for these values of $\tilde{\gamma}$ the amplitude instability essentially does not change as the phase amplitude instability domain moves to the right and crosses it.

If we enlarge the view and allow R and $\tilde{\alpha}_n$ to take larger values, we observe in Fig. 6 that a second amplitude instability domain appears in the right upper corner. This new instability domain exists if $\tilde{\gamma}$ is sufficiently large, moves to the left as $\tilde{\gamma}$ increases until $\tilde{\gamma} = 0.73704$, and then moves to the right.

Very interestingly, the lower boundary of that domain follows very closely the line $\tilde{\alpha}_n = \sqrt{\tilde{\gamma}} R$ which, in the limit $R \gg 1$, $X \gg 1$, is equivalent to $\tilde{\alpha}_n = 2\sqrt{\tilde{\gamma}}\sqrt{X} = 2\sqrt{\tilde{\gamma}}|f|$. Taking into account that $|f|$ is the Rabi frequency of the resonant mode scaled to $\sqrt{\gamma_\parallel \gamma_\perp}$ [see Eq. (12a)] and $\tilde{\gamma} = \gamma_\parallel/\gamma_\perp$, the product $\sqrt{\tilde{\gamma}}|f|$ represents the Rabi frequency scaled to $\gamma_\perp$. Since $\tilde{\alpha}_n$ is also the frequency of the side mode scaled to $\gamma_\perp$, we conclude that this second instability domain is associated with a resonance between a side mode and twice the Rabi frequency.

It is well known (see, e.g., Sec. 22-5 of Ref. [6]) that the Risken-Nummedal-Graham-Haken (RNGH) instability [2,3] in ring lasers is characterized by similar tongues of instability limited below by the Rabi frequency and above by the Rabi frequency multiplied by $\sqrt{2}$; see, e.g., Ref. [6]. Therefore, these secondary instability domains are the analog for a Fabry-Perot laser of the RNGH instability. We observe, however, that they exist only for extremely high values of the Rabi frequency, that could be achieved only if the laser is pumped

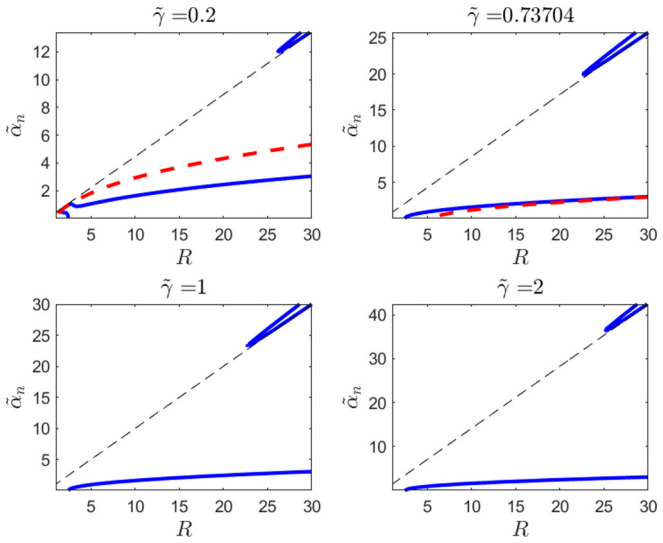

FIG. 6. Amplitude (solid blue line) and phase (dashed red line) instability domains in the plane $(R, \tilde{\alpha}_n)$ for the reported values of $\tilde{\gamma}$ and up to large values of R and $\tilde{\alpha}_n$. These plots show that a second amplitude instability domain appears with the shape of a narrow tongue leaning on the straight line $\tilde{\alpha}_n = \sqrt{\tilde{\gamma}}R$, displayed as a thin dashed black line.

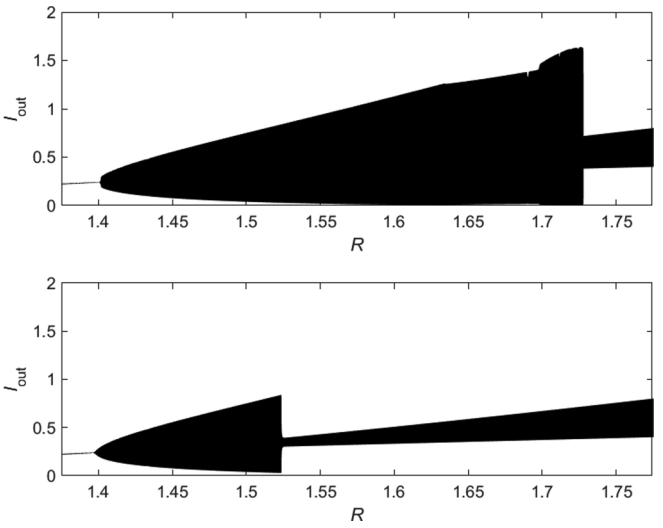

FIG. 7. Evolution of the total output intensity as R is varied from 1.375 to 1.775 (upper plot) and back (lower plot) with $\tilde{\gamma} = 0.1$ and $\tilde{\alpha}_1 = 0.5$. Correspondingly, the pump parameter varies from $A \approx 1.63$ to $A \approx 2.46$.

hundreds times above threshold. Precisely, the minimum instability threshold which is achieved for $\tilde{\gamma} = 0.73704$ is $R \approx 22.26$, which corresponds to $A \approx 259$. We can then conclude that *the pure* RNGH *instability in a Fabry-Perot laser does not exist*.

C. Numerical simulations of self-pulsing

Figures 3, 4, and 6 show the instability threshold of the single-mode solution with respect to the side mode with frequency $\tilde{\alpha}_n$. Depending on the cavity length, the instability will arise when the instability threshold is crossed by increasing the pump R for a particular modal index n. The instability is triggered by a symmetric pair of side modes but then by four-wave mixing processes it will involve other modes, giving rise to multimode dynamical regimes. Our analysis suggests that different kinds of self-pulsing will be observed associated with amplitude and phase instability.

In order to study the self-pulsing behavior that arises from the amplitude and phase instabilities and the competition between the two, we have numerically integrated the Maxwell-Bloch equations (26) and (27) with $\tilde{\gamma} = 0.1$. The instability domains are those shown in the left upper graph of Fig. 3. We have then chosen the value $\tilde{\alpha}_1 = 0.5$ for the scaled free spectral range and varied slowly the pump parameter in such a way that R varies linearly from 1.375 to 1.775 and returns. In that way, the two boundaries of the instabilities domain are crossed when they are very close one to the other and we expect to observe the effects of both instabilities. The ratio $k/\gamma_\perp$, which must be small for our analysis to hold, has been taken equal to 0.01. Only the electric field has been expanded in modes, and the expansion was truncated to 21 modes, 10 for each side of the spectrum; the variables P and D have not been expanded in modes. The total integration time, forward and backward, was 2×10^8 in units of $\gamma_\perp^{-1}$.

In the upper and lower plots of Fig. 7, we show the evolution of the output intensity as a function of R in the forward and backward scan, respectively.

In the forward scan, we see that, according with the stability analysis of Fig. 3, the single-mode solution becomes unstable at about $R = 1.4$ (with a small delay due to the inertia of the medium). The amplitude of the pulses increases with R until the self-pulsing solution undergoes a bifurcation at about $R = 1.64$ and the amplitude of the pulses increases more slowly; then, at about $R = 1.7$, another bifurcation occurs and the amplitude of the pulses acquires a modulation until it diminishes abruptly at about $R = 1.73$.

In the backward scan, the small amplitude self-pulsing persists until about $R = 1.5$, where there is an abrupt switch to the large amplitude self-pulsing. Therefore, there is a large range of R (and of the pump parameter) where the small-amplitude self-pulsing coexists with the large-amplitude self-pulsing in its three different forms.

These results can be compared to those of Ref. [32], where a similar scan forward and backward of the pump was performed. Our choice of the free-spectral range $\tilde{\alpha}_1 = 0.5$ is closer to the case of very short cavity studied in that paper. While bistability was also found in Ref. [32], we observe that in Ref. [32] the bistability is between the self-pulsing and continuous wave (cw) solutions, whereas in our simulations it is between two types of self-pulsing.

The details of the self-pulsing solutions for different values of R are illustrated in the four subfigures of Fig. 8. Each subfigure contains six graphs. The two graphs on the left show the time evolution of the mode intensities (upper graph) and of the total output intensity (lower graph); the two numbers above this figure are the minimum and maximum values of the intensity. The four graphs on the right show, from left to right, in the upper row the intensity spectrum and the relative phase $\phi_n(t) + \phi_{-n}(t) - 2\phi_0$ scaled to π, and in the lower row

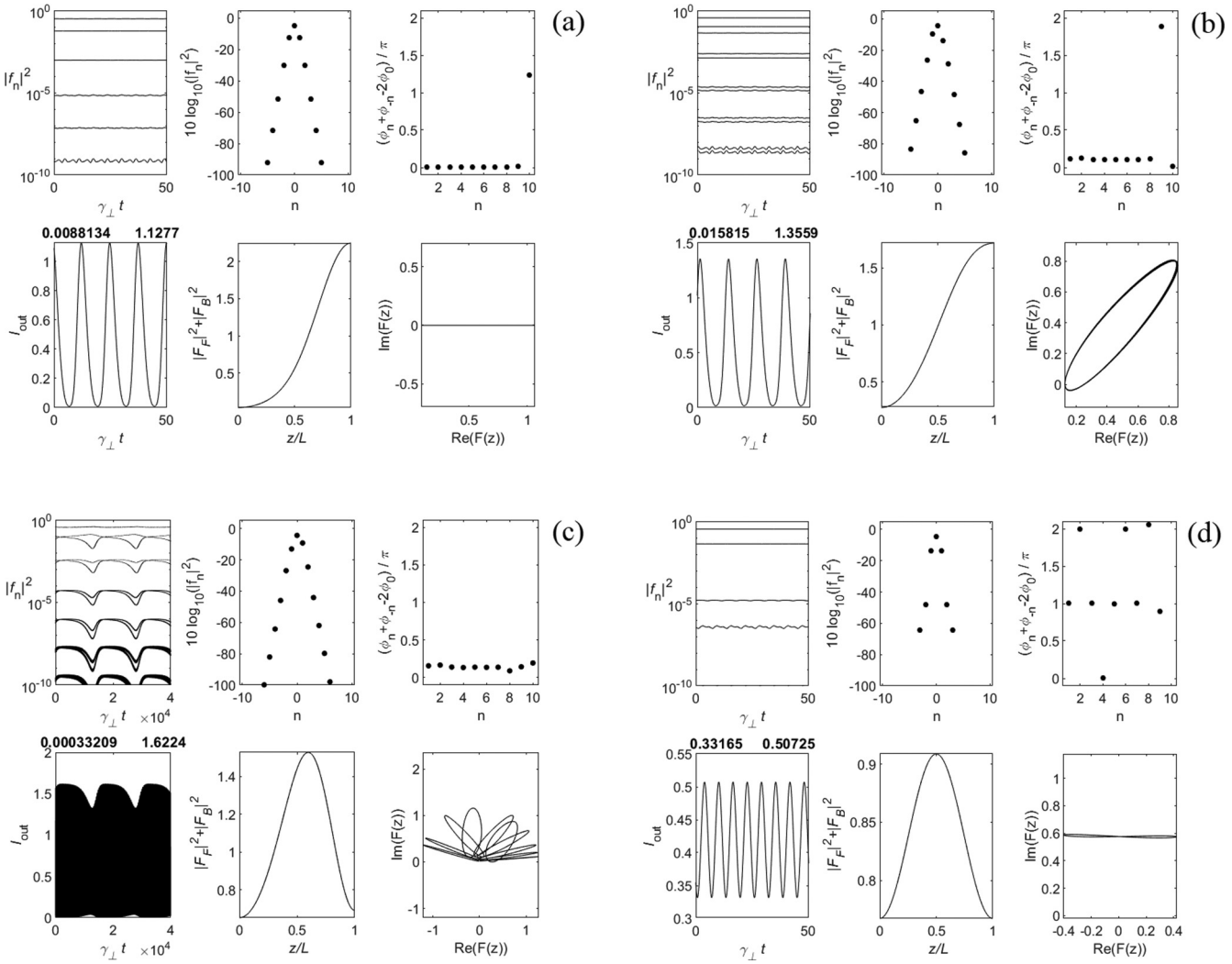

FIG. 8. Steady-state behavior for $\tilde{\gamma} = 0.1$, $\tilde{\alpha}_1 = 0.5$, and $R = 1.60$ ($A = 2.08$) (a), $R = 1.68$ ($A = 2.2512$) (b), $R = 1.72$ ($A = 2.3392$) (c), and $R = 1.60$ ($A = 2.08$) (d). Panels (a) to (c) refer to the forward scan of Fig. 7, and panel (d) to the backward scan. In each subfigure, the two graphs on the left show the time evolution of the mode intensities (upper graph) and of the total output intensity (lower graph), and four graphs on the right show, from left to right, in the upper row the intensity spectrum and the relative phase $\phi_n(t) + \phi_{-n}(t) - 2\phi_0$ scaled to π, and in the lower row the intensity profile along the cavity in the final state and the trajectory described by the tip of the electric field vector as we move along the cavity.

the intensity profile along the cavity in the final state, and the trajectory described by the tip of the electric field vector as we move along the cavity.

Figures 8(a), 8(b), and 8(c) refer to the forward scan and have been obtained, respectively, with $R = 1.60$, $R = 1.68$, and $R = 1.72$; Fig. 8(d) refers to the backward scan with $R = 1.60$. In each figure, the steady-state regime is shown after the transient evolution.

As we will see from the following analysis, Figs. 8(a) and 8(d) display, respectively, pure amplitude and pure phase self-pulsing, which are both stable for the same value of $R = 1.60$. Although the oscillating regime originated from the phase instability looks more like a smooth intensity modulation rather than a sequence of pulses, for brevity we speak of self-pulsing, with large or small amplitude, for both oscillating regimes.

The pure amplitude self-pulsing shown in Fig. 8(a) is characterized by constant mode intensities, deep modulation of the intensity with period equal to $2\pi/\tilde{\alpha}_1$, triangular intensity spectrum, relative phases locked to 0, spatial period of the intensity profile equal to twice the sample length, and real electric field.

The pure phase self-pulsing shown in Fig. 8(d) is characterized by constant mode intensities, moderate modulation of the intensity with period equal to $\pi/\tilde{\alpha}_1$, almost triangular intensity spectrum but with the three central modes with comparable intensities, relative phases locked to π for the odd modes and to 0 for the even modes, spatial period of the intensity profile equal to the sample length, and complex electric field.

In Figs. 8(a), 8(b), and 8(d), the relative phases associated with higher order modes sometimes do not respect the rule of locking at 0 or π, but this is only due to the fact that those modes have such small amplitudes that they are strong influenced by noise.

The differences between the two self-pulsing states can be understood considering three modes, the resonant one and its

first neighbors [25]. We can write the three complex amplitudes as $f_i(t) = \rho_i e^{i\phi_i(\tau)}$, $i = -1, 0, 1$. Since $\rho_1 = \rho_{-1}$ and all the three real amplitudes are constant as well as the phase ϕ_0, we can write the total electric field as

$$\begin{aligned} F(\tau) &= \rho_0 e^{i\phi_0} + \rho_1 e^{i\phi_1(\tau)} + \rho_1 e^{i\phi_{-1}(\tau)} \\ &= e^{i\phi_0}\{\rho_0 + \rho_1[e^{i\phi_1(\tau)-i\phi_0} + e^{i\phi_{-1}(\tau)-i\phi_0}]\}. \end{aligned} \tag{77}$$

In the presence of an amplitude instability, the side modes are locked to 0 and we have $\phi_1(\tau) - \phi_0 = -\phi_{-1}(\tau) + \phi_0$ or else $\phi_1(\tau) + \phi_{-1}(\tau) - 2\phi_0 = 0$ and

$$\begin{aligned} F(\tau) &= e^{i\phi_0}\{\rho_0 + \rho_1[e^{i\phi_1(\tau)-i\phi_0} + e^{-i\phi_1(\tau)+i\phi_0}]\} \\ &= e^{i\phi_0}\{\rho_0 + 2\rho_1 \cos[\phi_1(\tau) - \phi_0]\}. \end{aligned} \tag{78}$$

Since mode 1 has frequency α_1 its phase varies approximately as $\phi_1(\tau) = \phi_{10} + \alpha_1\tau$, if we neglect terms of order k. We can set $\phi_{10} - \phi_0 = 0$ by redefining the time and write the field intensity as

$$\begin{aligned} |F(\tau)|^2 &= \rho_0^2 + 4\rho_0\rho_1 \cos(\alpha_1\tau) + 4\rho_1^2 \cos^2(\alpha_1\tau) \\ &= \rho_0^2 + 2\rho_1^2 + 4\rho_0\rho_1 \cos(\alpha_1\tau) + 2\rho_1^2 \cos(2\alpha_1\tau). \end{aligned} \tag{79}$$

The intensity oscillates with period $2\pi/\alpha_1$ between $(\rho_0 - 2\rho_1)^2$ and $(\rho_0 + 2\rho_1)^2$. Correspondingly, the spatial period of the intensity profile is $2\bar{L}$.

If instead the single-mode solution is unstable for a phase instability, the side modes are locked to π and we have $\phi_1(\tau) - \phi_0 = -\phi_{-1}(\tau) + \phi_0 + \pi$ or else $\phi_1(\tau) + \phi_{-1}(\tau) - 2\phi_0 = \pi$ and the electric field is

$$\begin{aligned} F(\tau) &= e^{i\phi_0}\{\rho_0 + \rho_1[e^{i\phi_1(\tau)-i\phi_0} - e^{-i\phi_1(\tau)+i\phi_0}]\} \\ &= e^{i\phi_0}\{\rho_0 + 2i\rho_1 \sin[\phi_1(\tau) - \phi_0]\}. \end{aligned} \tag{80}$$

In this case, the electric field is intrinsically complex and the field intensity is

$$\begin{aligned} |F(\tau)|^2 &= \rho_0^2 + 4\rho_1^2 \sin^2(\alpha_1\tau) \\ &= \rho_0^2 + 2\rho_1^2 - 2\rho_1^2 \cos(2\alpha_1\tau), \end{aligned} \tag{81}$$

and it oscillates with period π/α_1 between ρ_0^2 and $\rho_0^2 + 4\rho_1^2$. Correspondingly, the spatial period of the intensity profile is $\bar{L}$. The amplitude of the oscillations is larger in the former case than in the latter. For instance, if $\rho_1 = \rho_0/2$ the intensity oscillates between 0 and $4\rho_0^2$ in the case of the amplitude instability and between ρ_0^2 and $2\rho_0^2$ in the case of the phase instability.

Figures 8(b) and 8(c) show more complex states that arise from an instability of the pure amplitude instability state.

In Fig. 8(b), the intensities of symmetric modes are no longer equal and the spectrum is asymmetric. The modes on the left side of the spectrum have larger intensities but the opposite situation is also possible, depending on the initial fluctuations. The modes are locked to a phase which is close to 0 but not exactly 0 and the trajectory in the complex plane resembles an ellipse.

In Fig. 8(c), the intensities of symmetric modes not only differ but they slowly oscillate in time. The period of these oscillations is about 15 000 scaled time units and this further slow modulation produces an alternation between the state where the modes on the right and left sides of the spectrum have larger intensities. This also causes a slow modulation in the total intensity and a rotation and deformation of the trajectory in the complex plane. Here, at difference with Figs. 8(a), 8(b), and 8(d) we have shown the time evolution on a much longer interval of time.

V. THE LORENZ-HAKEN INSTABILITY OF THE FABRY-PEROT LASER

In the case of a ring cavity, there is a general connection between single-mode and multimode instabilities in the sense that the existence of a single-mode instability implies the existence of a multimode instability and that the instability threshold is the same [6,34]. Here we show that this is not the case for a FP cavity. Let us consider the set of Eqs. (43) for $n = 0$ (resonant mode)

$$\begin{aligned} \frac{d\delta\tilde{f}_0(\tau)}{d\tau} &= -k\Bigg[(1 + i\theta)\delta\tilde{f}_0(\tau) \\ &\quad - \frac{A}{2\pi}\int_{-\pi}^{+\pi} d\varphi e^{-i\varphi}\delta\tilde{p}_0(\varphi, \tau)\Bigg], \end{aligned} \tag{82a}$$

$$\begin{aligned} \frac{d\delta\tilde{f}_0^*(\tau)}{d\tau} &= -k\Bigg[(1 - i\theta)\delta\tilde{f}_0^*(\tau) \\ &\quad - \frac{A}{2\pi}\int_{-\pi}^{+\pi} d\varphi e^{i\varphi}\delta\tilde{p}_0^*(\varphi, \tau)\Bigg], \end{aligned} \tag{82b}$$

$$\begin{aligned} \gamma_\perp^{-1}\frac{\partial\delta\tilde{p}_0(\varphi, \tau)}{\partial\tau} &= 2\cos\varphi[d(\varphi)\delta\tilde{f}_0(\tau) + f\delta\tilde{d}_0(\varphi, \tau)] \\ &\quad - (1 + i\Delta)\delta\tilde{p}_0(\varphi, \tau), \end{aligned} \tag{82c}$$

$$\begin{aligned} \gamma_\perp^{-1}\frac{\partial\delta\tilde{p}_0^*(\varphi, \tau)}{\partial\tau} &= 2\cos\varphi[d(\varphi)\delta\tilde{f}_0^*(\tau) + f^*\delta\tilde{d}_0(\varphi, \tau)] \\ &\quad -(1 - i\Delta)\delta\tilde{p}_0^*(\varphi, \tau), \end{aligned} \tag{82d}$$

$$\begin{aligned} \gamma_\parallel^{-1}\frac{\partial\delta\tilde{d}_0(\varphi, \tau)}{\partial\tau} &= -\cos\varphi[p^*(\varphi)\delta\tilde{f}_0 + p(\varphi)\delta\tilde{f}_0^* \\ &\quad + f\delta\tilde{p}_0^*(\varphi, \tau) + f^*\delta\tilde{p}_0(\varphi, \tau)] \\ &\quad - \delta\tilde{d}_0(\varphi, \tau), \end{aligned} \tag{82e}$$

where we have considered also the equations for $\delta\tilde{f}_0^*$ and $\delta\tilde{p}_0^*$. If we set

$$\delta\tilde{f}_0(\tau) = e^{\lambda\tau}\delta f_0, \tag{83a}$$

$$\delta\tilde{f}_0^*(\tau) = e^{\lambda\tau}\delta f_0^*, \tag{83b}$$

$$\delta\tilde{p}_0(\varphi, \tau) = e^{\lambda\tau}\delta p_0(\varphi), \tag{83c}$$

$$\delta\tilde{p}_0^*(\varphi, \tau) = e^{\lambda\tau}\delta p_0^*(\varphi), \tag{83d}$$

$$\delta\tilde{d}_0(\varphi, \tau) = e^{\lambda\tau}\delta d_0(\varphi), \tag{83e}$$

the equations for $\delta p_0(\varphi)$, $\delta p_0^*(\varphi)$, and $\delta d_0(\varphi)$ are

$$\begin{aligned} 0 &= -\lambda\delta p_0(\varphi) - \gamma_\perp(1 + i\Delta)\delta p_0(\varphi) \\ &\quad + 2\gamma_\perp\cos\varphi[d(\varphi)\delta f_0 + f\delta d_0(\varphi)], \end{aligned} \tag{84a}$$

$$\begin{aligned} 0 &= -\lambda\delta p_0^*(\varphi) - \gamma_\perp(1 - i\Delta)\delta p_0^*(\varphi) \\ &\quad + 2\gamma_\perp\cos\varphi[d(\varphi)\delta f_0^* + f\delta d_0(\varphi)], \end{aligned} \tag{84b}$$

$$\begin{aligned} 0 &= -(\lambda + \gamma_\parallel)\delta d_0(\varphi) + \gamma_\parallel\cos\varphi \\ &\quad \times[p^*(\varphi)\delta f_0 + p(\varphi)\delta f_0 + f\delta p^*(\varphi) + f^*\delta p(\varphi)], \end{aligned} \tag{84c}$$

In the ring cavity case, the correspondence between single-mode and multimode instabilities is a consequence of the circumstance that the set of algebraic equations for $\delta\tilde{p}_0$, $\delta\tilde{p}_0^*$, $\delta\tilde{d}_0$ for the single-mode instability coincide with the set of algebraic equations for $\delta\tilde{p}_n$, $\delta\tilde{p}_n^*$, $\delta\tilde{d}_n$ if in the former λ is replaced by $-i\tilde{\alpha}_n$. In the case of an FP cavity, Eqs. (84) with that substitution do not coincide with Eqs. (45a), (46b), and (45b), respectively, because of the different dependence on the fast spatial variable φ.

We focus on the resonant case $\Delta = \theta = 0$ and on the amplitude instability, which in the ring cavity is known as the Lorenz-Haken instability. Hence, we can set $\delta f_0^* = \delta f_0$ and $\delta p_0^*(\varphi) = \delta p_0(\varphi)$ and we obtain a simple expression for $\delta p_0(\varphi)$:

$$\delta p_0(\varphi) = \frac{2\cos\varphi}{1+4X\cos^2\varphi} \times \frac{\tilde{\lambda}+\tilde{\gamma}-4\tilde{\gamma}X\cos^2\varphi}{(\tilde{\lambda}+1)(\tilde{\lambda}+\tilde{\gamma})+4\tilde{\gamma}X\cos^2\varphi}\delta f_0, \quad (85)$$

with $\tilde{\lambda} = \lambda/\gamma_\perp$ and $X = f^2$. When we insert the above expression for $\delta p_0(\varphi)$ in Eq. (82a) with $\theta = 0$, we get an equation for $\tilde{\lambda}$,

$$\tilde{\lambda} = \tilde{k}[AH(\tilde{\lambda}, X\tilde{\gamma}) - 1], \quad (86)$$

with $\tilde{k} = k/\gamma_\perp$ and

$$H(\tilde{\lambda}, X, \tilde{\gamma}) = \frac{1}{2\pi}\int_{-\pi}^{\pi} d\varphi \frac{2\cos^2\varphi}{1+4X\cos^2\varphi} \times \frac{\tilde{\lambda}+\tilde{\gamma}-4\tilde{\gamma}X\cos^2\varphi}{(\tilde{\lambda}+1)(\tilde{\lambda}+\tilde{\gamma})+4\tilde{\gamma}X\cos^2\varphi}. \quad (87)$$

The integral can be calculated analytically and the result is given in Appendix B. By a squaring operation, we obtain finally a characteristic equation of sixth order in $\tilde{\lambda}$

$$\sum_{n=0}^{6} a_n\tilde{\lambda}^n = 0, \quad (88)$$

with real coefficients a_n which depend on R, $\tilde{k}$, and $\tilde{\gamma}$ and whose explicit expressions are written in Appendix B.

The boundary of the instability domain can be found by setting $\tilde{\lambda} = -i\omega$. By equating separately the real and imaginary parts of the equation and eliminating by successive steps the frequency ω, we obtain the equation

$$\mathcal{F}(R, \tilde{k}, \tilde{\gamma}) = p_1^2 - p_2 p_3 = 0, \quad (89)$$

with

$$p_1 = a_1^2 a_6 - a_1 a_2 a_5 + a_0 a_3 a_5, \quad (90a)$$

$$p_2 = a_1 a_2 a_3 - a_0 a_3^2 - a_1^2 a_4 + a_0 a_1 a_5, \quad (90b)$$

$$p_3 = a_1 a_4 a_5 - a_0 a_5^2 - a_1 a_3 a_6. \quad (90c)$$

The Lorenz-Haken instability in an FP laser was studied previously in Refs. [35,36] but, to the best of our knowledge, an analytic expression for the boundary of the instability domain was never given. The condition $\mathcal{F}(R, \tilde{k}, \tilde{\gamma}) = 0$ can be studied in the plane of two of the three parameters with the third fixed. In Fig. 9, we show the instability domains in the plane $(\tilde{\gamma}, \tilde{k})$

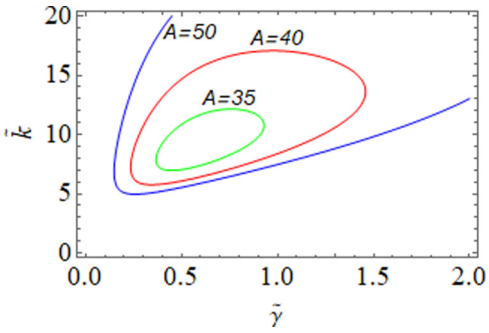

FIG. 9. Instability domain for the single-mode instability of a FP laser in the plane $(\tilde{\gamma}, \tilde{k})$ for the indicated values of the pump parameter A. No instability exists for $A \lesssim 33.4$.

with R fixed which amounts to fixing the pump parameter A. The instability domain shrinks to a point as A diminishes. The point has coordinates $\tilde{\gamma} = 0.583441$ and $\tilde{k} = 8.95482$ and the minimum value of the pump parameter for which the instability exists is $A = 33.3695$.

VI. CONCLUSIONS

In this paper, we have extended the traveling wave formalism of Ref. [28] to the case of a Fabry-Perot cavity where the two-level medium does not fill the cavity. This allows us to model, for instance, FP lasers with an external cavity. We observe, however, that in the model the total cavity length Λ appears just in the expression for the modal frequencies [Eq. (35)]. Therefore, two FP cavities with the same Λ and different lengths of the active medium are equivalent.

In the limit of population variables much faster than the electric field, we have derived the linearized equations suitable to analyze the stability of the single-mode solution for both active and passive resonators driven by an external coherent field. We have focused on the active case and we have assumed that the atomic frequency coincides with one cavity frequency, so that the instabilities that arise split in a natural way in amplitude and phase instabilities.

We have considered both the case in which the ratio $\tilde{\gamma} = \gamma_\parallel/\gamma_\perp$ is substantially smaller than unity and the case that $\tilde{\gamma}$ is of order unity. It turns out that the multimode Fabry-Perot instability arises near threshold only when $\tilde{\gamma}$ is significantly smaller than unity, a result that joins perfectly with the analysis of Ref. [33] that was performed in the limit of adiabatic elimination of the atomic polarization fluctuations only. We have studied the self-pulsing behavior that arises from the multimode instability for $\tilde{\gamma}$ substantially smaller than unity and have found self-pulsations generated by the amplitude instability and self–pulsations generated by the phase instability. It turns out that there is a hysteretic behavior between the two of them when the pump parameter is swept forward and backward and the difference between the two regimes has been analyzed with the help of a simple three-mode model.

Although our model is strictly valid for a two-level medium, we believe that it gives useful insights also for other kind of lasers such as QCLs. It is true that two ingredients typical of those lasers are missing, namely carrier diffusion and the linewidth enhancement factor [19]. Yet, we observe

that the linewidth enhancement factor is very often neglected even in treatments especially devoted to a QCL [21–25] and that due to the fast recovery time of a QCL carrier diffusion is not able to wash out completely the grating, contrary to what happens in diode lasers. As a consequence, the inclusion of carrier diffusion in models where population inversion is described by the zeroth- and second-order spatial harmonics simply implies that the recovery time for the latter is slightly smaller than for the former. We do not believe that our results would be strongly modified by the inclusion of carrier diffusion.

On the other hand, with respect to Refs. [21–25], our analysis is valid even when the laser is not very close to threshold, and this discloses new scenarios. For instance, our instability conditions $\mathcal{G}_{\pm}(\tilde{\alpha}_n, R, \tilde{\gamma}) > 1$ coincide with those of Ref. [25] expressed by Eq. (27) of that paper at first order in the stationary intensity X, but they are valid for any value of X and of the pump A. This allowed us to discover phenomena such as the existence of a critical value for the pump above which the amplitude instability exists even in the limit $\tilde{\alpha}_n \to 0$ as the phase instability and a critical value for $\tilde{\gamma}$ above which the amplitude instability has a lower threshold than the phase instability. Moreover, we were able to find an instability tongue which exists for very large values of the pump that we interpret as the true analog of the RNGH instability in a FP laser, because it is associated with a resonance between the side-mode frequency and the Rabi frequency. The amplitude instability that occurs for smaller pump values is instead due to spatial hole burning.

Very recently, we have become aware that the procedure of doubling the length of a Fabry-Perot cavity in order to introduce traveling modes was utilized in Ref. [37]. In that article, however, the procedure is illustrated in two Appendixes and is used only to derive a single-mode model, without considering multimode aspects.

ACKNOWLEDGMENTS

We are grateful to Massimo Brambilla for useful suggestions about the bistability of amplitude and phase instability and to Marco Piccardo for informations about the parametric values in Fabry-Perot quantum cascade lasers.

APPENDIX A

The functions $H_1(\tilde{\alpha}_n, X, \tilde{\gamma})$ and $H_2(\tilde{\alpha}_n, X, \tilde{\gamma})$ defined by Eqs. (58) can be written as

$$H_1(\tilde{\alpha}_n, X, \tilde{\gamma}) = \frac{\mathcal{N}_1(\tilde{\alpha}_n, X, \tilde{\gamma})}{\mathcal{D}(\tilde{\alpha}_n, \tilde{\gamma})}, \tag{A1}$$

$$H_2(\tilde{\alpha}_n, X, \tilde{\gamma}) = \frac{i(2 - i\tilde{\alpha}_n)}{2X^2} \frac{\mathcal{N}_2(\tilde{\alpha}_n, X, \tilde{\gamma})}{\mathcal{D}(\tilde{\alpha}_n, \tilde{\gamma})}, \tag{A2}$$

with

$$\mathcal{N}_1(\tilde{\alpha}_n, X, \tilde{\gamma}) = \frac{2\tilde{\alpha}_n(1 - i\tilde{\alpha}_n) + i\tilde{\gamma}(2 - 3i\tilde{\alpha}_n)}{\sqrt{1 + 4X}} - i\tilde{\gamma}(2 - i\tilde{\alpha}_n)S(\tilde{\alpha}_n, X, \tilde{\gamma}), \tag{A3}$$

$$\begin{aligned}\mathcal{N}_2(\tilde{\alpha}_n, X, \tilde{\gamma}) &= \tilde{\alpha}_n^2 + i\tilde{\alpha}_n(1 + \tilde{\gamma}) - \tilde{\gamma}\frac{1 + 2X}{\sqrt{1 + 4X}} \\ &\quad - \left[\tilde{\alpha}_n^2 + i\tilde{\alpha}_n(1 + \tilde{\gamma}) - \tilde{\gamma}(1 + 2X)\right]S(\tilde{\alpha}_n, X, \tilde{\gamma}),\end{aligned} \tag{A4}$$

$$\mathcal{D}(\tilde{\alpha}_n, \tilde{\gamma}) = 2\tilde{\alpha}_n(1 - i\tilde{\alpha}_n)(1 + \tilde{\gamma} - i\tilde{\alpha}_n), \tag{A5}$$

and

$$\begin{aligned}S(\tilde{\alpha}_n, X, \tilde{\gamma}) &= \sqrt{\frac{(1 - i\tilde{\alpha}_n)(\tilde{\gamma} - i\tilde{\alpha}_n)}{(1 - i\tilde{\alpha}_n)(\tilde{\gamma} - i\tilde{\alpha}_n) + 4\tilde{\gamma}X}} \\ &= S_+(\tilde{\alpha}_n, R, \tilde{\gamma}) - iS_-(\tilde{\alpha}_n, R, \tilde{\gamma}),\end{aligned} \tag{A6}$$

with $S_{\pm}(\tilde{\alpha}_n, R, \tilde{\gamma})$ given by Eqs. (69)–(71).

APPENDIX B

The function $H(\tilde{\lambda}, X, \tilde{\gamma})$ defined by Eq. (87) is given by

$$H(\tilde{\lambda}, X, \tilde{\gamma}) = \frac{(\tilde{\lambda} + 2)(\tilde{\lambda} + \tilde{\gamma})}{2\tilde{\lambda}(\tilde{\lambda} + \tilde{\gamma} + 1)X}\sqrt{\frac{(\tilde{\lambda} + 1)(\tilde{\lambda} + \tilde{\gamma})}{(\tilde{\lambda} + 1)(\tilde{\lambda} + \tilde{\gamma}) + 4\tilde{\gamma}X}} - \frac{\tilde{\lambda} + 2\tilde{\gamma} + (\tilde{\lambda} + \tilde{\gamma} + 1)\sqrt{1 + 4X}}{2\tilde{\lambda}(\tilde{\lambda} + \tilde{\gamma} + 1)X\sqrt{1 + 4X}}. \tag{B1}$$

The coefficients of the sixth-order characteristic equation (88) are

$$a_0 = -4\tilde{k}^2\tilde{\gamma}^2 - 4\tilde{k}^2\tilde{\gamma}^2R + 8\tilde{k}^2\tilde{\gamma}^2R^2, \tag{B2}$$

$$a_1 = 4\tilde{k}^2\tilde{\gamma}^2 - 4\tilde{k}^2\tilde{\gamma}(2 + \tilde{\gamma})R + 4\tilde{k}\tilde{\gamma}(\tilde{k} + \tilde{\gamma})R^2 + 4\tilde{k}^2\tilde{\gamma}(1 + \tilde{\gamma})R^3, \tag{B3}$$

$$a_2 = 4\tilde{k}\tilde{\gamma}(\tilde{k} + \tilde{\gamma} + 1) - \tilde{k}^2\tilde{\gamma}^2 + 3\tilde{k}^2\tilde{\gamma}^2R - 2\tilde{k}\tilde{\gamma}^2R^2 + 4\tilde{k}\tilde{\gamma}(\tilde{k} + \tilde{\gamma} + 1)R^3, \tag{B4}$$

$$a_3 = -2\tilde{k}\tilde{\gamma}(\tilde{k} + \tilde{\gamma} - 1) + 4\tilde{k}(1 + \tilde{\gamma})^2R + 4\tilde{k}^2(2 + 3\tilde{\gamma})R - \tilde{\gamma}(2\tilde{k} + \tilde{\gamma} + 1)R^2 + \tilde{\gamma}(4\tilde{k} + \tilde{\gamma} + 1)R^3, \tag{B5}$$

$$a_4 = -\tilde{k}^2 - (1 + \tilde{\gamma})^2 - 2\tilde{k}(1 + \tilde{\gamma}) + 3\tilde{k}^2R + 8\tilde{k}(1 + \tilde{\gamma})R + (1 + \tilde{\gamma})^2R - \tilde{\gamma}R^2 + \tilde{\gamma}R^3, \tag{B6}$$

$$a_5 = -2(\tilde{k} + \tilde{\gamma} + 1) + 2(2\tilde{k} + \tilde{\gamma} + 1)R, \tag{B7}$$

$$a_6 = -1 + R. \tag{B8}$$

[1] C. L. Tang, H. Statz, and G. deMars, J. Appl. Phys. **34**, 2289 (1963).
[2] H. Risken and R. Nummedal, J. Appl. Phys. **39**, 4662 (1968).
[3] R. Graham and H. Haken, Z. Phys. **213**, 420 (1968).
[4] H. Haken, in *Laser Theory*, edited by S. Flugge and L. Genzel, Handbuch der Physik Vol. 25 (Springer-Verlag, Berlin, 1970).
[5] S. Sargent III, M. Scully, and W. Lamb, *Laser Physics* (Addison-Wesley, Reading, MA, 1974).
[6] L. Lugiato, F. Prati, and M. Brambilla, *Nonlinear Optical Systems* (Cambridge University Press, Cambridge, UK, 2015).
[7] P. Del'Haye, A. Schliesser, O. Arcizet, T. Wilken, R. Holzwarth, and T. J. Kippenberg, Nature (London) **450**, 1214 (2007).
[8] T. Herr, V. Brasch, J. D. Jost, C. Y. Wang, N. M. Kondratiev, M. L. Gorodetsky, and T. J. Kippenberg, Nat. Photon. **8**, 145 (2014).
[9] Y. K. Chembo, Nanophotonics **5**, 214 (2016).
[10] A. Hugi, G. Villares, S. Blaser, H. C. Liu, and J. Faist, Nature (London) **492**, 229 (2012).
[11] Q. Y. Lu, M. Razeghi, S. Slivken, N. Bandyopadhyay, Y. Bai, W. J. Zhou, M. Chen, D. Heydari, A. Haddadi, R. McClintock, M. Amanti, and C. Sirtori, Appl. Phys. Lett. **106**, 051105 (2015).
[12] J. Faist, G. Villares, G. Scalari, M. Rösch, C. Bonzon, A. Hugi, and M. Beck, Nanophotonics **5**, 272 (2016).
[13] M. Piccardo, P. Chevalier, T. S. Mansuripur, D. Kazakov, Y. Wang, N. A. Rubin, L. Meadowcroft, A. Belyanin, and F. Capasso, Opt. Express **26**, 9464 (2018).
[14] M. Piccardo, B. Schwarz, D. Kazakov, M. Beiser, N. Opačak, Y. Wang, S. Jha, J. Hillbrand, M. Tamagnone, W. T. Chen, A. Y. Zhu, L. L. Columbo, A. Belyanin, and F. Capasso, Nature (London) **582**, 360 (2020).
[15] M. Homar, J. V. Moloney, and M. San Miguel, IEEE J. Quantum Electron. **32**, 553 (1996).
[16] E. Gehrig, O. Hess, A. Volland, G. Jennemann, I. Fischer, and W. Elsäßer, J. Opt. Soc. Am. B **21**, 1638 (2004).
[17] P. Bardella, L. L. Columbo, and M. Gioannini, Opt. Express **25**, 26234 (2017).
[18] N. Vukovic, J. Radovanovic, V. Milanovic, and D. L. Boiko, Opt. Quantum Electron. **52**, 91 (2020).
[19] C. Silvestri, L. L. Columbo, M. Brambilla, and M. Gioannini, Opt. Express **28**, 23846 (2020).
[20] N. Vukovic, J. Radovanovic, V. Milanovic, and D. L. Boiko, Opt. Quantum Electron. **48**, 254 (2016).
[21] A. Gordon, C. Y. Wang, L. Diehl, F. X. Kärtner, A. Belyanin, D. Bour, S. Corzine, G. Höfler, H. C. Liu, H. Schneider, T. Maier, M. Troccoli, J. Faist, and F. Capasso, Phys. Rev. A **77**, 053804 (2008).
[22] J. Bai, IEEE Trans. Nanotechnol. **11**, 292 (2012).
[23] T. S. Mansuripur, C. Vernet, P. Chevalier, G. Aoust, B. Schwarz, F. Xie, C. Caneau, K. Lascola, C. E. Zah, D. P. Caffey, T. Day, L. J. Missaggia, M. K. Connors, C. A. Wang, A. Belyanin, and F. Capasso, Phys. Rev. A **94**, 063807 (2016).
[24] N. N. Vukovic, J. Radovanovic, V. Milanovic, and D. L. Boiko, IEEE J. Sel. Top. Quantum Electron. **23**, 1200616 (2017).
[25] Y. Wang and A. Belyanin, Phys. Rev. A **102**, 013519 (2020).
[26] D. C. Cole, A. Gatti, S. B. Papp, F. Prati, and L. Lugiato, Phys. Rev. A **98**, 013831 (2018).
[27] D. Burghoff, Optica **7**, 1781 (2020).
[28] L. A. Lugiato and F. Prati, Phys. Scr. **93**, 124001 (2018).
[29] H. J. Carmichael, Opt. Commun. **53**, 122 (1985).
[30] L. A. Lugiato and L. M. Narducci, Z. Phys. **71**, 129 (1988).
[31] A. Hugi, R. Maulini, and J. Faist, Semicond. Sci. Technol. **25**, 083001 (2010).
[32] N. N. Vukovic. J. V. Radovanovic, V. B. Milanovic, A. V. Antonov, D. I. Kuritsyn, V. V. Vaks, and D. L. Boiko, arXiv:1902.00205.
[33] L. A. Lugiato and F. Prati, Phys. Rev. Res. **1**, 032029(R) (2019).
[34] L. A. Lugiato and L. M. Narducci, Phys. Rev. A **32**, 1576 (1985).
[35] P. Chenkosol and L. W. Casperson, J. Opt. Soc. Am. B **10**, 817 (1993).
[36] J. L. Font, F. Silva, and R. Vilaseca, Opt. Commun. **138**, 403 (1997).
[37] J. F. Mercier and J. V. Moloney, Phys. Rev. E **66**, 036221 (2002).